Marginal zone B cells are antigenically activated, infiltrate the kidneys, and exacerbate angiotensin II-dependent hypertension in mice

Hericka B. Figueiredo Galvao[1,2†], Maria Jelinic[1,2,3†], Maggie Lieu[1,2], Vivian Tran[1,2], Buddhila Wickramasinghe[1,2], Jake N. Robertson[1,2], Tayla A. Gibson Hughes[1,2], Henry Diep[1,4], Asha Haslem[5], Mathew G. Lewsey[5,6,7,8], Alexander Bobik[3,9,10], Christopher G. Sobey[1,2,3], Tomasz J. Guzik[11,12], Grant R. Drummond[1,2,3*#], Antony Vinh[1,2#].

[1] Centre for Cardiovascular Biology and Disease Research (CCBDR), La Trobe Institute for Molecular Science (LIMS), La Trobe University, Melbourne, VIC, Australia

[2] Department of Microbiology, Anatomy, Physiology and Pharmacology, School of Agriculture, Biomedicine and Environment, La Trobe University, Melbourne, VIC, Australia

[3] Baker Heart and Diabetes Institute, Melbourne, VIC, Australia

[4] Victorian Heart Institute, Monash University, Melbourne, VIC, Australia

[5] La Trobe Institute for Sustainable Agriculture and Food, AgriBio, La Trobe University, Melbourne, Victoria, Australia

[6] Australian Research Council Centre of Excellence in Plants for Space, AgriBio, La Trobe University, Melbourne, Victoria, Australia

[7] Australian Research Council Research Hub for Protected Cropping, AgriBio, La Trobe University, Melbourne, Victoria, Australia

[8] La Trobe Institute for Molecular Sciences, La Trobe University, Melbourne, Victoria, Australia

[9] Department of Immunology, Monash University, Melbourne, VIC, Australia

[10] Centre for Inflammatory Diseases, Monash University, Melbourne, VIC, Australia

[11] Centre for Cardiovascular Sciences, University of Edinburgh, Edinburgh, UK.

[12] Department of Medicine and Omicron Medical Genomics Laboratory, Jagiellonian University, Collegium Medicum, Kraków, Poland.

*Corresponding author:

Prof. Grant R. Drummond

Centre for Cardiovascular Biology and Disease Research, La Trobe Institute for Molecular Science (LIMS)

Department of Microbiology, Anatomy, Physiology & Pharmacology

School of Agriculture, Biomedicine and Environment, La Trobe University

Victoria 3086, Australia

T: +61 3 9479 5843

E: g.drummond@latrobe.edu.au

† Equal first author contribution

Equal senior author contribution

Running title: Marginal zone B cells are antigenically activated in hypertension

Abstract

B cells are key contributors to hypertension, but the specific subsets involved and whether their activation is antigen-dependent remain unclear. Here, we show angiotensin II infusion in male and female mice induces hypertension and selectively expands marginal zone B (MZB) cells. Using single-cell multiomic sequencing (RNA+VDJ) and high-dimensional flow cytometry we show MZB cells exhibit increased expression of the antigen-specific activation marker Nur77, undergo clonal expansion, and are enriched for IGHV1 B cell receptor variants. Activated and memory MZB cells also accumulate in the kidneys of hypertensive mice. Importantly, hypertensive responses to angiotensin II infusion were significantly blunted in mice lacking MZB cells (BAFF-R$^{-/-}$), highlighting a causal role for MZB cells in disease development. These findings identify MZB cells as the major activated B cell subset in hypertension and suggest that targeting MZB cells or the (auto)antigens that activate them may offer a novel approach for treating hypertension.

Introduction

The immune system plays a crucial role in the development of cardiovascular diseases including hypertension [1]. Clinical studies from over 50 years ago linked hypertension with B cell activation, evidenced by elevated circulating IgG antibodies [2-5]. More recently, preclinical studies in experimental models of hypertension have shown that B cell depletion – either genetically or pharmacologically – reduces blood pressure elevation. These interventions also limit cardiac and vascular remodelling, suggesting a causal role for B cells in hypertension and its sequalae [6-8].

The previous findings imply that B cells could be a target for future anti-hypertensive therapies. However, global B cell depletion is unlikely to be clinically viable due to its detrimental effects on immune function and infection control. A more targeted approach, such as selectively inhibiting the specific B cell subsets that are activated in hypertension, would likely improve clinical translation. To date, no studies have identified the specific subpopulation(s) of B cells driving hypertension or described the mechanisms underlying their activation.

Mature B cells originate from one of two lineages. The B-1 lineage - which includes B-1a and B-1b B cells - is the first to develop, appearing during foetal development [9, 10]. B-1a and B-1b cells respond to T cell-independent antigens through one of two main mechanisms: (1) activation of innate cell surface immune receptors such as toll-like receptors, in type 1 T cell-independent responses [11-13]; or (2) recognition of highly conserved pathogenic epitopes or sequences by B cell receptors (BCRs) in type 2 T cell-independent responses [14]. The B-2 lineage, which includes follicular (FO) and marginal zone (MZB) B cells, develops postnatally following the hematopoietic switch from the foetal liver to the bone marrow [15-17]. FO B cells are primarily activated by antigens binding to their BCRs and require co-stimulation from T

cells to exert their full response [18]. In contrast, MZB cells are more versatile, capable of responding to both T cell-independent or T cell-dependent antigens [19-23].

With the exception of B-1a cells [9], successful B cell activation typically leads to clonal expansion. When this activation is antigen-specific, the resulting B cells express identical BCRs – also known as B cell clones. This process reduces overall BCR diversity and skews the repertoire toward specific immunoglobulin heavy chain variable regions (IGHVs) [24].

In this study, we used single-cell transcriptomics, BCR sequencing and high-dimensional flow cytometry to determine which B cell subsets are activated during the development of angiotensin II-dependent hypertension in mice, and to uncover the mechanisms involved. We observed that MZB cells were selectively expanded in the spleens of hypertensive mice and a higher proportion of MZB cells expressed markers of activation. Activated MZB-like cells also accumulated in the kidneys of hypertensive mice, where they exhibited a memory phenotype. Mice deficient in MZB cells (BAFF-R$^{-/-}$ mice) were protected from hypertension, indicating a causal role for MZB cells. Finally, MZB expansion in hypertension was accompanied by clonal BCR expansion and an over-representation of IGHV1 BCR variants, consistent with antigen-dependent activation. These findings identify MZB cells as key mediators of hypertension and provide a foundation for future studies aimed at uncovering the antigens responsible for MZB cell activation.

Methods

Animals and ethics

Male and female C57BL6 mice aged 8- to 11-weeks were sourced from the La Trobe Animal Research and Teaching Facility (LARTF; Bundoora, Australia) and Monash Animal Services (Clayton, Australia). B cell activating factor-receptor knockout (BAFF-R$^{-/-}$) mice were bred and housed in the Animal Research laboratories (Clayton, Australia) and LARTF (Bundoora,

Australia). Mice were housed in temperature (22 ± 2°C) and humidity (55 ± 15%) regulated rooms with 12-hour light/dark cycles in individually ventilated cages (IVC) with access to food and water *ad libitum*. All procedures were approved by the La Trobe University Animal Ethics Committee (AEC 16-93), the Monash University Animal Research Platform Ethics Committee (MARP/2016/077) and the Institutional Biosafety Committee (GM16-25). All experiments were performed in accordance with the Australian Code for the Care and Use of Animals for Scientific Purposes (8th Edition 2013, updated 2021).

Induction of hypertension

Mice were randomly assigned to hypertensive or normotensive groups. Hypertension was induced via subcutaneous infusion of angiotensin II (0.7 mg/kg/day) using osmotic minipumps (Alzet Model 2004, USA). Control mice received vehicle (0.1% acetic acid in saline). Infusions were maintained for either 14 or 28 days, as previously described ([25]). Following pump implantation, mice were allowed to recover in warmed, clean IVC cages containing only littermates of the same sex and treatment group.

Systolic blood pressure recordings

Systolic blood pressure (SBP) was measured using tail-cuff plethysmography (MC4000 Multichannel System; Hatteras Instruments, USA), as previously described [26]. Briefly, mice were acclimated to the procedure on two separate occasions prior to baseline recordings. SBP was recorded weekly for 14 or 28 days following osmotic minipump implantation. Only clear, artefact-free traces were included in analyses. To minimize stress-induced variability, male and female mice were recorded separately on the same day.

Tissue collection and sample preparation

Bone marrow, spleen, blood and kidney samples were harvested from vehicle- and angiotensin II-infused mice for preparation into single-cell solutions. Mice were euthanised by

carbon dioxide asphyxiation, followed immediately by cardiac puncture to collect blood samples after administration of enoxaparin sodium (100 µL; 400 IU; Clexane®, Auckland, NZ). Mice were then perfused with phosphate buffered saline (PBS), and tissues were collected in ice cold sterile PBS.

Bone marrow was flushed from femoral and tibial bones and spleens were mechanically dissociated. Samples were then passed through 70 µm sterile cell strainers and treated with red blood cell (RBC) lysis buffer (0.15 M NH_4Cl, 0.01 M $KHCO_3$, 6.0 mM EDTA, dH_2O) for 5 min at room temperature. Blood samples were centrifuged at 2,000x *g* for 10 min at 4°C. The plasma was removed, and the cell pellet was resuspended in RBC lysis buffer for 5 min, twice. Live cell counts were obtained using trypan blue exclusion and a Countess™ Automated Cell Counter (Invitrogen). Final suspensions were adjusted to 10^7 live cells/mL in PBS and kept on ice until downstream processing.

Kidneys were halved, minced with scissors and digested in PBS containing collagenase type XI (0.16 mg/mL), collagenase type I-S (0.18 mg/mL) and hyaluronidase (0.03 mg/mL; Sigma-Aldrich, USA) for an hour at 37°C. Digested tissue was passed through a 70 µm filter, centrifuged at 450x *g* for 10 min at 4°C and resuspended in 40% isotonic Percoll™ solution (GE Healthcare Life Science, UK). A 60% Percoll™ underlay was added, and samples were centrifuged at 1385x *g* for 25 min at 25°C (no brakes). Mononuclear cells were collected from the interface, washed with PBS, and resuspended for flow cytometry.

High-dimensional flow cytometry

Single-cell suspensions were loaded onto 96-well microplates. Live cells were stained with LIVE/DEAD™ Fixable Blue Dead Cell Stain (1:1000 dilution in PBS; ThermoFisher Scientific) for 15 min at 4°C. Samples were then washed with FACS buffer (0.5% bovine serum albumin (BSA; Sigma-Aldrich, USA) in PBS), spun and resuspended in a cocktail of fluorescently

labelled antibodies against cell surface markers for 25 min at 4°C (**Supplementary Table 1)**. Single-stain controls were prepared from spleen and bone marrow aliquots.

Cells were fixed, and permeabilized using eBioscience™ Fixation/Permeabilization Diluent (Invitrogen) for 30 minutes at 4°C. After washing with permeabilization buffer, cells were stained with intracellular antibodies (**Supplementary Table 1**) for 15 min at room temperature. Final washes were performed, and cells were resuspended in 1% formalin in FACS buffer and stored at 4°C until analysis.

Flow cytometry was performed using a BD FACSSymphony™ A3 analyser (BD Bioscience, San Jose, CA, USA) using the FACSDiva software v9. Data quality was ensured by removing events with unstable acquisition or flow rate using FlowAI [27] in FlowJo v10.10.0. Cleaned FCS files containing only live, non-myeloid cells were batch-corrected using the cyCombine workflow [28] with logicle transformation (flowWorkspace, R package, “estimateLogicle” function) [29]. Batch corrected files were gated in FlowJo v10.10.0 and population counts were exported for statistical analyses. Gating strategies and population summaries are provided in **Supplementary Table 2**.

Single-cell multiomic (RNA+VDJ) sequencing

Staining and sorting

Bone marrow and spleen samples were harvested from 28 day-infused mice (n=12 per tissue) for single-cell RNA sequencing (scRNAseq) and single-cell V(D)J sequencing (scVDJseq). Each group included 3 male and 3 female mice infused with either vehicle or angiotensin II (**Supplementary Fig. 1**). Samples were dissociated into single-cell suspensions under DNAse- and RNAse-free conditions and loaded onto 96-well microplates, including additional wells for unstained and compensation controls.

Cells were incubated with Fc block (1:500 dilution in FACS buffer, BioLegend, USA) for 5 min at room temperature. Sample indexing was achieved using cell surface hashtags (TotalSeq™-C; BioLegend, USA), diluted to 1:2000 in FACS buffer and centrifuged at 14,000 × g for 10 min at 4°C to remove antibody conjugates. Each sample was incubated with a unique hashtag for 30 min at room temperature, followed by staining with an antibody master mix for fluorescence-activated cell sorting (FACS). This included markers for nucleated (Vybrant™ DyeCycle™ Ruby^{+}, 1:500 dilution) metabolically active (Calcein AM Blue^{+}, 1:500 dilution) and live (SYTOX™ green^{-}, 1:1000 dilution, added immediately prior to sorting) cells (all from ThermoFisher Scientific). Supplementary tables 3 and 4 describe the antibodies, dyes and hashtags used for single-cell sequencing.

Spleen samples were additionally stained with anti-CD19 (PE-Cy7, 1:500) and anti-CD23 (PE, 1:500) antibodies to enrich for B-1 cells (CD19^{+}CD23^{-}), which are a minor splenic B cell population [30]. After staining and washing, samples were filtered through 40 µm sterile cell strainers and kept on ice prior to sorting.

For spleens, live, nucleated, metabolically active CD19^{+}CD23^{-} B cells were sorted into one tube, and all other viable cells were sorted into a second tube. These were then combined to double the B-1 cell proportion. For bone marrow, all viable cells were sorted into a single tube. Sorted cells were centrifuged at 450x *g* for 10 min at 4°C and resuspended in FACS buffer. Cell counts were manually measured using trypan blue stain and a hemocytometer.

Samples from the same treatment group were pooled together at equal quantities and final manual cell counts were performed. Each pool contained 3 male and 3 female samples of the same tissue type. Pooled samples were placed on ice and immediately processed for single-cell RNA sequencing (scRNAseq) and single-cell V(D)J sequencing (scVDJseq) at the Genomics Platform, La Trobe University.

Sequencing and library preparation

Gel-Bead-in-Emulsion (GEM) generation was performed using the Chromium Next GEM Chip G (PN-1000127) and Chromium controller (10X Genomics, VIC, AUS). Libraries were prepared using the Chromium Next GEM Single Cell 5′ Kit v2 (PN-1000265) and sequenced on a NovaSeq Illumina system (Illumina, Scoresby, VIC, AUS).

Gene expression libraries were generated using the CellRanger v7.0 multi-library pipeline (10X Genomics), mapped to the mouse mm10 reference transcriptome. This yielded 12 count matrices across bone marrow and spleen samples. FASTQ files were reconstructed from these matrices, and BCR sequences were extracted using sample-specific barcodes and mapped to the GRCm38 Mouse V(D)J Reference 7.0.0.

Pre-processing

CellRanger outputs were used to generate per-sample Seurat objects in R (version 4.2.1), annotated with treatment, sex and animal number metadata. Mitochondrial gene expression and cell cycle scores were calculated using the Seurat package (v4.1.1), using “PercentageFeatureSet” and “CellCycleScoring” functions, respectively [31-33]. Cells with <200 genes or >10% mitochondrial gene expression were excluded. Doublets were identified using DoubletFinder (v2.0.3), assuming a ~6.1% doublet rate based on ~1.2×10^4 loaded cells per group [34] .

Normalisation, dimension reduction and clustering

Bone marrow (VEH: 5,551 cells; ANG: 5,117 cells) and spleen cells (VEH:8,366 cells; ANG: 6,997 cells) expressed an average of 2,151 and 1,627 genes with average gene counts of 9,086 and 4,202, respectively (**Supplementary Fig. 2**). Raw RNA counts were normalised

using SCTransform (SCT), excluding mitochondrial gene expression and cell cycle phase from regression.

Principal component analysis (PCA) was performed on SCT-normalised data, and the first 30 PCA vectors were used for Louvain-based t-distributed stochastic neighbour embedding (tSNE) and uniform manifold approximation and projection (UMAP) graph reductions. Cells were then clustered into populations using a standard resolution of 0.8.

To improve community detection, Leiden-based clustering was performed using Monocle3 (v1.2.9) on raw and SCT-normalised counts [35-38]. UMAP and tSNE reduction graphs were generated, and clusters were defined using automatic resolution selection. Cluster robustness was validated using Seurat (v4.1.1), requiring $\geq$3 differentially expressed genes per cluster. Final Monocle3 cluster assignments, UMAP and tSNE embeddings were then transferred to the original Seurat object for downstream analyses.

Cell-type annotations

Cell-type predictions were performed using SingleR (v1.10.0) [39] and reference data from the Immunological Genome Project via the celldex (v1.6.0) package [39]. The top 200 differentially expressed genes (log fold change $\geq$ 0.25) were used for label assignment. Predicted labels were manually confirmed or revised using known transcript markers from the literature.

Pseudotime trajectory inference and GO analyses

To investigate transcriptional differentiation during B cell maturation pseudotime trajectory analysis was performed using Monocle3. An unsupervised principal graph was constructed via reversed graph embedding of transcriptomic data, allowing cells to be ordered along a trajectory and assigned pseudotime values. This approach captured dynamic changes in gene

expression associated with B cell maturation and enabled downstream differential gene expression analyses.

Spatial autocorrelation analysis in Monocle3 was used to identify genes that varied significantly along the pseudotime trajectory. Genes with a “Moran’s I” q-value < 0.05 were considered significantly variable and grouped into modules using a resolution of 0.001. Gene sets were retrieved from the Molecular Signature Database via the msigdbr package (v7.5.1)[40, 41], and GO enrichment analysis was performed using the clusterProfiler package (v4.4.4) [42, 43], applying a similarity cutoff of 0.5 and a q-value threshold of < 0.05. Selected GO terms were visualised using ggplot2 (v3.5.1)[44]; full results are provided in **Supplementary files 3,4**.

Immune receptor repertoire analyses

To identify B cell populations with shared B cell receptor (BCR) sequences, transcriptional data were integrated with antigen receptor sequencing (scVDJseq). Productive/functional BCRs from bone marrow and spleen B cells were identified using the Immcantation framework (Docker container) [45, 46]. BCRs contain three complementarity-determining regions (CDRs), with CDR1 and CDR2 involved in MHC recognition and CDR3 conferring antigen specificity [47].

Thus, BCR clonotypes were defined via unsupervised spectral clustering of BCR sequences based on V and J gene similarity using the scoper (v1.2.1) [48, 49] package. Diversity and species richness metrics were calculated and visualised using the alakazam (v1.2.1) [50] package. Scaled frequencies of variable (V) gene segments from immunoglobulin heavy (IGH) and immunoglobulin light kappa/lambda (IGK/IGL) chains were extracted using scRepertoire

(v1.7.2) [51] and analysed via two-way ANOVA with Tukey's *post-hoc* test to detect biases in V region usage.

Statistical analyses

Power calculations determined that a minimum sample size of n = 9 was required to detect a 25% change in mean SBP with a standard deviation of 10%, 80% power and α = 5%.

For bioinformatics analyses, differentially expressed genes ($\log_2$(fold change) $\geq$ 0.25 and expressed by $\geq$ 10% of cells [52]) were analysed using Wilcoxon rank-sum tests comparing each cluster to all others. Genes with a Bonferroni-adjusted $p \leq 0.01$ were considered significant. For cell type predictions via SingleR, differentially expressed genes were evaluated using a Wilcoxon rank-sum test (with adjusted $p < 0.05$). For GO enrichment significance was assessed using the Benjamini-Hochberg correction ($q < 0.05$).

Physiological data distribution was assessed using the D'Agostino & Pearson test, and outliers were identified using a ROUT method (false discovery rate = 1%). SBP data were analysed using a two-way mixed effects model with Geisser-Greenhouse correction and Tukey's multiple comparisons test. Flow cytometry data were analysed using a two-tailed unpaired t-tests. For sex- or genotype-specific analyses, SBP datasets were analysed using a three-way mixed effects model with Geisser-Greenhouse correction, followed by Tukey's *post hoc* test. All other physiological data were analysed using a two-way ANOVA followed by Tukey's *post hoc* test.

All physiological data analyses were performed using GraphPad Prism 9.4.0 (GraphPad Software, San Diego, California, USA). Results were considered statistically significant $p < 0.05$. Physiological data are presented as the mean ± standard error of the mean (SEM).

Results

Single-cell transcriptomics captures all stages of B cell development

Single-cell suspensions of bone marrow and spleen from male and female mice infused with either angiotensin II or vehicle were subjected to transcriptomic sequencing. Following data cleaning and normalisation, cells were analysed for identity, function, and B cell receptor (BCR) clonotype profiling. B cells were identified based on expression of established marker genes (*Cd79a, Cd79b, Ebf1, Cd74, Vpreb3, Ly6d, Bank1*)[52-55], comprising ~15% of bone marrow and ~42% spleen cells (**Supplementary Fig. 2**). While several non-B cell populations were also identified (**Supplementary Fig. 3,4**), they were not the focus of the present study. B cells were further classified into subpopulations, each defined by at least 3 differentially expressed marker genes (**Fig. 1a-c**). In total, 15 B cell populations were identified across bone marrow and spleen samples (**Fig. 1d**).

Ly6d is recognised as one of the earliest markers of B cell specification [56]. Its low expression in the pre-pro B, pro-B and pre-B cell receptor dependent (pre-BCRd) populations indicates their recent commitment to a B cell fate (**Fig. 1a**). The transcription factor *Ebf1* directs B cell development by downregulating myeloid genes (e.g. *Tyrobp* and *Clec12a*) and upregulating B cell-specific genes [57-59]. Consistent with their recent commitment to a B cell fate, pre-pro B cells had remnant expression of *Tyrobp* and *Clec12a* (data not shown) and lower levels of the pan B cell markers *Cd19* and *Cd79a*, compared to other B cells (**Fig. 1a**).

The pro-B cell stage is characterised by upregulation of recombination-activating genes, *Rag1* and *Rag2,* which initiate the expression of the BCR heavy chains associated with surrogate light chains [60-62]. Thus, pro-B cells were identified by their expression of *Rag1*, *Rag2* and the BCR surrogate light chains *Vpreb1*, *Vpreb2* and *Vpreb3* (**Fig. 1a**). Tonic activity from the pre-BCR provides survival and proliferation cues to large pre-B cells, which undergo several rounds of cell division [60]. These large pre-B cells were annotated as the pre-BCRd

population, characterised by the expression of immature BCR surrogate light chains (**Fig. 1a**) and proliferation-associated genes (*Mki67*, *Pclaf* and *Top2a*) [52, 63, 64] (**Fig. 1b**).

Large pre-B cells differentiate into small pre-B cells in which BCR light chain rearrangement takes place following reduced interleukin-7 (IL-7) signalling, which epigenetically permits light chain recombination [65-68]. We identified two small pre-B cell populations: pre-BCR-independent-1 (pre-BCRi 1) and pre-BCR-independent-2 (pre-BCRi 2). Both populations lacked proliferative gene expression but expressed low levels of mature BCR light chain genes (*Iglc1*, *Iglc2* and *Iglc3*), indicating ongoing light chain rearrangement (**Fig. 1b**).

Consistent with their immature phenotypes, the IL7 receptor (*Il7r*) was enriched in pro-B, pre-BCRd and pre-BCRi 1 populations. *IL7r* expression was absent in mature B cells and lower in the pre-BCRi 2 population, suggesting a more differentiated state (**Fig. 1b**). B cell progenitors with a newly formed mature BCR undergo central tolerance checking in the bone marrow as transitional B cells, annotated here as Tr1 [69, 70]. During this process, Tr1 survival is dependent on B cell activating factor (BAFF)-mediated stimulation of the BAFF receptor (*Tnfrsf13c*) [71, 72]. Accordingly, Tr1 cells expressed *Tnfrsf13c* and high levels of *Cd24a*, a common marker of transitional B cells (CD24; **Fig. 1b**) [52].

Tr1 that pass central tolerance checkpoints in the bone marrow migrate to the spleen for peripheral tolerization and maturation [69, 70]. Transitional B cells in the spleen (Tr2) closely resembled Tr1 cells in the bone marrow, as evidenced by their shared expression of transcriptional regulators (**Fig. 1a-c**) and top uniquely expressed genes (**Fig. 1d**). Mature B cells, including follicular B-2 (FO B-2), marginal zone B cells (MZB), circulating B-2, B-1 B cells, germinal centre (GC), memory (Bmem) and plasma cell (PC) populations were also identified in our dataset.

Circulating B-2 cells found in the bone marrow lacked expression of immature markers such as surrogate light chains (**Fig. 1a**) and expressed *Fcer2a* (CD23), a B-2 lineage B cell marker (**Fig. 1c**). Circulating B-2 cells had a similar gene expression profile to FO B-2 cells in the spleen, which are characterised by the expression of *Fcer2a*, *Cr2* (CD21) and the *Klf2* transcription factor, known to maintain the follicular phenotype (**Fig. 1c,d**) [73].

MZB cells were distinguished by the expression of *Cr2* and *Mzb1* (Marginal zone B and B1 cell-specific protein) [74], with low levels of *Klf2* and *Fcer2a* (**Fig. 1c,d)**. B-1 cells were identified by enriched *Mzb1* expression and the absence of B-2 lineage markers, consistent with their distinct developmental origin and functional profile (*Fcer2a* and *Cr2*) (**Fig. 1c**).

During germinal centre (GC) reactions, activated FO B-2 and MZB cells receive co-stimulatory signals from T cells and differentiate into either memory B cells or plasma cells. Here, we identified a small population of GC cells expressing proliferation markers (*Mki67*, *Pclaf* and *Top2a;* **Fig. 1b**) and activation-induced cytidine deaminase (*Aicda;* **Fig. 1c**), which initiates somatic hypermutation and class-switch recombination of BCRs [75].

Memory B cell (Bmem) differentiation is promoted by the transcription factor *Bach2*, which suppresses plasma cell transcriptional programming [76]. The Rac regulator, *Dock2,* is also essential for Bmem formation [77]. Indeed, we identified a population of B cells expressing high levels of *Bach2* and *Dock2,* consistent with Bmem cells (**Fig. 1d**). Plasma cells (PCs) are professional antibody-secreting cells. Upon terminal differentiation, PCs downregulate virtually all classical B cell lineage markers [78]. PC populations in both spleen and bone marrow lacked expression of *Ebf1, Cd19, Ms4a1* and *Tnfrsf13c* (**Fig. 1a-c**), but expressed the plasma cell-specific B cell maturation antigen receptor (BCMA; *Tnfrsf17*) and transcription factor B lymphocyte-induced maturation protein 1 (*Prdm1*; Blimp-1; **Fig. 1c**) [52, 79, 80]. An additional

distinct population of mature B cells expressing interferon-stimulated genes, including *Ifit3, Isg15, Irf7* (**Fig. 1f**)[81-85], was tentatively annotated as anti-viral B cells [86].

Pseudotime analysis supports B cell subtype classification

To corroborate B cell subtype identification, a three-dimensional pseudotime trajectory was generated (**Fig. 2a**). Genes expressed along the trajectory were grouped into modules for gene ontology (GO) analyses (**Fig. 2b-d**). Module 6 was enriched in Pre-BCRd and GC cells, with GO terms related to proliferation (*DNA replication*, *microtubule binding*, *nuclear division* and *chromosome segregation*; **Fig. 2c**), consistent with their proliferative phenotype and active cell cycling.

GC cells also expressed genes in module 12 (**Fig. 2d**), which is associated with *leukocyte cell-cell adhesion*, *signalling receptor activity*, *cytokine binding and regulation of leukocyte activation*, supporting their role in receiving co-stimulatory signals from T cells. Bmem cells expressed genes enriched for *epigenetic regulation of gene expression*, *chromatin remodelling* and the *maintenance of stem cell populations* (Module 3; **Fig. 2c**).

PCs were largely associated with *secretory pathways*, *protein folding* and *humoral immune responses*, all of which are essential for antibody secretion (Module 13; **Fig. 2d**) [87]. Finally, anti-viral B cells expressed GO terms associated with viral responses and interferon-mediated signalling (Module 14; **Fig. 2d**).

Expansion and activation of marginal zone B cells in chronically hypertensive mice

Angiotensin II infusion increased systolic blood pressure from a baseline of 119.8 ± 3.6 mmHg to 167.2±2.6 mmHg by day 28 (**Fig. 3a**). In contrast, there was no change in blood pressure across the 28 days in vehicle-infused control mice. Comparing our transcriptomic data across the two groups, the proportion of MZB cells in the spleens from hypertensive mice were

increased (21.5 ± 2.5% vs 16.8 ± 0.9% of sequenced splenic B cells; **Fig. 3b, c**). This expansion was confirmed by flow cytometry, which showed a higher frequency of MZB cells in the spleens from hypertensive mice (5.4 ± 0.3% vs 4.2 ± 0.2% of live spleen cells; **Fig. 3d**).

Since B cell activation precedes expansion, we measured expression of the general B cell activation marker CD69 and the BCR-specific activation marker Nur77, using flow cytometry. The expression of both CD69 and Nur77 was increased in MZB cells from hypertensive mice (**Fig. 3e,f**), compared to normotensive mice. Collectively, our findings identify MZB cells as the key B cell subtype activated in hypertension.

A comprehensive summary of all B cell populations analysed using flow cytometry of the spleen, bone marrow, blood and kidneys from normotensive and hypertensive mice is available in **Supplementary File 1**.

Marginal zone-like B cells accumulate in the kidneys and adopt a memory phenotype during chronic hypertension

MZB cells typically reside in the marginal sinus of the spleen. However, MZB-like populations have been previously recorded in inflamed tissues in autoimmune conditions like thyroiditis [88], diabetes [89] and systemic lupus erythematosus [90]. The kidneys are particularly relevant in hypertension, serving both as regulators of salt and water balance, and as a key target vulnerable to injury and dysfunction due to mechanical forces imposed by elevated pulse pressures [1]. Hence, we collected kidneys from mice to analyse the impact of hypertension on B cell populations using flow cytometry.

The percentage of total B cells in kidneys from hypertensive mice was almost double that in normotensive mice (2.5 ± 0.4% vs 1.4 ± 0.2% of live kidney cells; **Fig. 4a**). Most B cells in the kidneys were phenotypically similar to MZB cells in the spleen, expressing CD19, B220 and

CD21 with little to no expression of CD23 (**Fig. 4b**). Expression of the activation markers CD69 and Nur77 in these MZB-like cells was significantly elevated in hypertensive mice (**Fig. 4c, d**), indicating BCR-specific activation, similar to that observed in the spleen. Furthermore, the expression of the memory marker CD27 was increased, with three times more MZB-like memory cells in the kidneys of hypertensive mice compared to normotensive controls (**Fig. 4e**).

Antigen-specific adaptations of B cell receptors on marginal zone B cells in hypertension

The increased expression of Nur77 in MZBs in the spleen and kidneys suggests that these cells undergo antigenic activation in hypertension. Antigen-driven B cell activation typically reduces BCR diversity due to clonal expansion and preferential enrichment of specific BCR heavy chains with a higher affinity for the activating antigen, a phenomenon known as BCR skewing [24].

To investigate this, we used single-cell VDJ sequencing (BCR sequencing) to quantify BCR clones and BCR heavy chain expression to identify the BCRs that may be involved in detecting hypertension-specific antigens. Total BCR diversity and IgM diversity was reduced in MZBs in hypertensive mice according to Shannon Entropy and Simpsons index (**Fig. 5a, b**), which is consistent with antigen-dependent activation. Additionally, the number of BCR clones in the spleens from hypertensive mice was also increased (**Fig. 5c**).

Although antigen specificity and binding is encoded by all three complementarity-determining regions (CDR) of a BCR, the third CDR (CDR3) loop is the most diverse and is the main determinant of antigen specificity [47]. Comparative analysis of CDR3 amino acid sequences revealed 58 unique BCR clones in hypertensive mice that were absent in normotensive controls, either as expanded clones or unexpanded receptors (**Fig. 5d**). We then quantified

the percentage expression of each IGHV family from individual mice to determine if BCRs were skewed. Consistent with BCR skewing, hypertensive mice had significantly greater percentages of MZB cells with an IGHV1 BCR variant (**Fig. 5e**). Taken together, our transcriptomic, flow cytometry and BCR sequencing data provide converging evidence that MZB cells undergo antigen-dependent activation during hypertension. Furthermore, BCRs expressing IGHV1 variants likely play a central role in recognising the activating antigen(s) driving this response.

Chronic hypertension induces marginal zone B cell expansion and activation in both sexes

Pre-menopausal females are known to be less susceptible to developing hypertension and other cardiovascular diseases [91, 92]. To identify sex differences in the immune response to angiotensin II, we performed subgroup analyses comparing data from male and female mice. Angiotensin II infusion increased SBP in both sexes; however, the pressor response in female mice was delayed. In male mice, SBP peaked within 7 days of angiotensin II infusion (**Fig. 6a**). In contrast, SBP levels were lower in females compared to males at days 7 and 14 of angiotensin II infusion and peaked at day 21, at a level that was comparable with males (**Fig. 6a**). Cardiac hypertrophy, assessed by an increase in the ratio of heart weight to tibia length, was evident in male mice after 28 days of angiotensin II treatment, but absent in females (**Fig. 6b**).

Despite these physiological differences, MZB cell responses were remarkably similar across sexes. Indeed, both male and female mice exhibited similar magnitudes of MZB cell expansion, upregulation of activation markers CD69 and Nur77, and accumulation of memory MZB-like cells in the kidneys (**Fig. 6c**).

Beyond MZBs, sex-specific differences occurred in other B cell subsets. Female mice had higher baseline levels of total and activated antibody secreting cells in blood and bone marrow, as previously reported [93, 94] (**Supplementary File 2).** Moreover, angiotensin II treatment induced a greater increase in the percentage of B cells expressing CD9 in females compared to males (**Supplementary File 2**). CD9 is a marker of regulatory B cells [95-97].

Marginal zone B cell deficiency blunts the hypertensive response to angiotensin II

To investigate the causal role of marginal zone B (MZB) cells in hypertension, we used BAFF-R$^{-/-}$ mice, which are largely devoid of mature B cells subtypes including MZBs. BAFF-R$^{-/-}$ and wild type mice were treated with angiotensin II and B cell subsets and blood pressure responses were assessed. In wild type mice, angiotensin II increased the number of MZBs in the spleen (**Fig. 7a**). In contrast, MZBs were virtually absent in spleens from BAFF-R$^{-/-}$ mice, both under both basal (vehicle-treated) and hypertensive conditions (**Fig. 7a**). Consistent with a pathophysiological role for MZBs in hypertension, BAFF-R$^{-/-}$ mice displayed a blunted pressor response to angiotensin II (**Fig. 7b**).

Discussion

Accumulating evidences supports a pro-hypertensive role for B cells [6-8]. However, the specific B cell subsets driving immune/pressor responses and whether their activation is antigen-dependent remains unclear in the context of hypertension. Here we used single-cell multiomic (RNA+VDJ) sequencing and high-dimensional flow cytometry to comprehensively characterise B cell responses during angiotensin II-induced hypertension. We show that angiotensin II-dependent hypertension in both male and female mice is associated with antigen-dependent activation of MZBs in spleens and kidneys. Splenic MZBs were clonally expanded and memory MZB cells were detected in kidneys from hypertensive mice. Importantly, BAFF-R$^{-/-}$ mice, which are deficient in MZB cells, displayed an attenuated

hypertensive response to angiotensin II, implying a causal role for MZB cells in the development of hypertension.

MZB cells are a functionally versatile B cell population known to respond to both T cell-dependent and -independent antigens [19-23]. Thus, MZB cells can contribute to both innate and adaptive immune responses [21]. Activation of MZB cells is typically associated with the formation of IgM^+ memory B cells. However, MZB cells can also undergo class switching to produce IgG and IgA [22]. IgG3 secretion has traditionally been linked to T cell-independent activation, particularly in response to repetitive polysaccharide antigens and complement receptor signalling [98, 99]. IgA production likewise follows T cell-independent activation, but is driven by distinct innate stimuli such as lipopolysaccharide (LPS) and TGF-β [100]. We have previously shown that angiotensin II-dependent hypertension in mice is associated with elevated levels of IgG3 antibodies in the circulation and vascular tissues [7, 101] which may suggest that T cell-independent antigens are at least partially responsible for MZB cell activation in hypertension.

Activation of MZB cells leads to migration into the splenic follicle, where they can function as antigen presenting cells to follicular dendritic cells and follicular T cells [102, 103]. While MZB cells were traditionally considered to be confined to the spleen in mice but not humans [104-106], emerging evidence indicates their presence in other anatomical compartments in mice, including the bone marrow, where they localise around sinusoidal capillaries and contribute to T cell-independent responses to blood-borne antigens [107]. In autoimmune conditions, B cells with a MZB-like phenotype have been identified within inflamed tissues, exhibiting markers of activation and immunological memory [88-90]. In the present study, we identified MZB-like cells in the kidneys of hypertensive mice, characterised by the expression of activation and memory markers. This observation suggests these MZB cells are not only

activated in hypertension but may also migrate to renal tissues, a site where they have the potential to directly influence blood pressure regulation and contribute to the pathogenesis of hypertension [1]. Supporting this notion, previous work has shown that genetic depletion of B cells reduces renal expression of the vasopressin 2 receptor, implicating B cells in mechanisms of salt and water retention [8].

While the present study demonstrates that MZB cells are present and activated within hypertensive kidneys, the specific immunological functions through which they contribute to disease progression remain undefined. Three principal mechanisms merit consideration. First, MZB cells may produce antibodies that exacerbate vascular or renal dysfunction. Clinical and experimental models of hypertension consistently show elevated levels of IgG antibodies in circulation and within affected tissues. IgG accumulation may drive inflammation via Fc receptor-mediated macrophage activation or complement cascade engagement [1]. Notably, agonistic autoantibodies targeting angiotensin II type 1 [108-110] and endothelin-1 [111] receptors have been reported in hypertension and pre-eclampsia; however, whether MZB cells are the source of these autoantibodies remains unknown.

Second, MZB cells may contribute to disease via cytokine secretion. B cell-derived cytokines have been implicated in other inflammatory conditions — for example, tumour necrosis factor-alpha from B cells promotes plaque formation and instability in atherosclerosis [112], while interleukin-6 and interferon-gamma secretion drive T cell proliferation and Th17 polarisation in autoimmune diseases [113, 114].

Third, MZB cells may act as antigen-presenting cells, amplifying adaptive immune responses within hypertensive target organs. This role could be particularly relevant in the kidney, where sustained immune activation may contribute to tissue injury and fibrosis. Dissecting the relative

contribution of these pathways will be critical to elucidating the pathogenic role of MZB cells in hypertension and may inform the development of targeted immunotherapeutic strategies.

Regardless of the downstream mechanisms, our findings provide compelling evidence that MZB cells undergo antigen/BCR-dependent activation in the context of hypertension. Notably, expression of Nur77 – a well-established surrogate marker of BCR signalling [115] – was significantly elevated in splenic MZB cells from hypertensive mice compared to normotensive controls. This was accompanied by an expansion of BCR clones, with over half of all clones from hypertensive mice expressing heavy chain variable regions from the IGHV1 family. These data strongly implicate the emergence of (auto)antigens in hypertension that are selectively recognised by IGHV1-enriched BCRs on MZB cells.

Such antigen-specific activation suggests a mechanistic link between hypertension and autoreactive B cell responses. Importantly, this opens the possibility for targeted immunomodulatory strategies, such as antigen-specific tolerization, contingent upon the identification of the relevant (auto)antigens. Advances in *in silico* structural modelling – exemplified by platforms such as AlphaFold2 [116] and IgFold [117] – now enable high-resolution prediction of BCR-antigen interactions. Future studies could leverage these tools to model the structure of expanded IGHV1 BCRs, thereby facilitating the identification of putative pro-hypertensive antigens and informing the development of precision therapeutics.

Another important aspect of this study is the comparison of B cell responses between sexes. Although MZB responses to angiotensin II were broadly similar in males and females, we observed some notable differences. Most prominently, the increased expression of the regulatory molecule CD9 on B cells in female mice. CD9 is associated with IL-10-secretory regulatory B cells, which help temper immune activation [95-97]. Previous studies have shown that angiotensin II promotes CD9+ regulatory B cells via the type 1A receptor, and that

depletion of this receptor exacerbates atherosclerotic lesions [118]. Our findings align with this, showing CD9 upregulation across multiple B cell subsets, including MZB cells, following angiotensin II infusion. Interestingly, CD9 induction was more robustly induced in female mice, suggesting a heightened anti-inflammatory profile that may contribute to their relative resistance to hypertension and cardiac hypertrophy. However, this could also reflect lower basal BCR activation in female MZB cells, in which reduced antigen-specific activation could be playing a role in their protection.

In conclusion, this study identifies MZB cells as the principal B cell subset that is activated and expanded in angiotensin II-induced hypertension. We provide the first evidence of hypertension-specific BCRs within this compartment, notably enriched for IGHV1 family sequences. These findings implicate MZB cells in antigen-driven immune responses that may contribute to disease progression. Crucially, they open new avenues for therapeutic intervention—particularly through the identification of pro-hypertensive (auto)antigens and the development of antigen-specific tolerization strategies. Advances in structural modelling platforms, offer promising tools to predict BCR-antigen interactions and accelerate the discovery of pathogenic targets. Together, our findings establish MZB cells as key immunological players in hypertension and lay the foundation for precision immunotherapies aimed at restoring cardiovascular homeostasis.

Funding

This study was funded by NHMRC Ideas Grants (GNT2003752 and GNT2020452; G.R.D., M.J., T.J.G. and A.V.) and the La Trobe ABC Internal Investment Scheme (M.J., G.D. and A.V.). M.J. was supported by a joint NHMRC and NHF Postdoctoral Fellowship (GNT1146314 & 101943). H.F.G., M.L., V.T., B.W., J.N.R. and T.A.G.H. were supported by

Australian Research Training Scholarships. J.N.R. was also supported by a Defence Science Institute Research Higher Degree Student Grant.

Author contributions

Conceptualization: H.F.G., M.J., G.R.D., A.V.; Methodology (flow cytometry and multiomic sequencing): H.F.G., M.J., M.L., A.V., A.H., M.G.L.; Methodology (tissue preparation): H.F.G., M.J., M.L., V.T., B.W., J.N.R., T.A.G.H., H.D., A.V.; Methodology (surgeries and blood pressures): H.F.G., M.L., H.D.; Formal analysis: H.F.G. and A.V.; Writing (original draft): H.F.G.; Writing (review and editing): M.G.L, M.J., A.B., C.G.S., T.J.G., G.R.D., A.V.

Acknowledgements

We acknowledge: the Bioimaging Platform, La Trobe University for flow cytometry; the Genomics Platform, La Trobe University for single-cell sequencing services; and the La Trobe Animal Research and Teaching Facility staff for their assistance with animal husbandry. Schematic figures were created with BioRender.com.

Conflict of interest

None declared.

Code availability

The code used in this study is publicly available through the individual package documentation files.

References

1. Drummond, G.R., et al., *Immune mechanisms of hypertension*. Nat Rev Immunol, 2019. **19**(8): p. 517-532.
2. Ebringer, A. and A.E. Doyle, *Raised serum IgG levels in hypertension*. Br Med J, 1970. **2**(5702): p. 146-8.

3. Gudbrandsson, T., et al., *Immunological changes in patients with previous malignant essential hypertension*. Lancet, 1981. **1**(8217): p. 406-8.
4. Suryaprabha, P., T. Padma, and U.B. Rao, *Increased serum IgG levels in essential hypertension*. Immunol Lett, 1984. **8**(3): p. 143-5.
5. Hilme, E., et al., *Increased secretion of immunoglobulins in malignant hypertension*. J Hypertens, 1989. **7**(2): p. 91-5.
6. Mathis, K.W., et al., *Preventing autoimmunity protects against the development of hypertension and renal injury*. Hypertension, 2014. **64**(4): p. 792-800.
7. Chan, C.T., et al., *Obligatory Role for B Cells in the Development of Angiotensin II-Dependent Hypertension*. Hypertension, 2015. **66**(5): p. 1023-33.
8. Dingwell, L.S., et al., *B-Cell Deficiency Lowers Blood Pressure in Mice*. Hypertension, 2019. **73**(3): p. 561-570.
9. Baumgarth, N., *The double life of a B-1 cell: self-reactivity selects for protective effector functions*. Nat Rev Immunol, 2011. **11**(1): p. 34-46.
10. Godin, I.E., et al., *Para-aortic splanchnopleura from early mouse embryos contains B1a cell progenitors*. Nature, 1993. **364**(6432): p. 67-70.
11. Crampton, S.P., E. Voynova, and S. Bolland, *Innate pathways to B-cell activation and tolerance*. Ann N Y Acad Sci, 2010. **1183**: p. 58-68.
12. Bekeredjian-Ding, I. and G. Jego, *Toll-like receptors--sentries in the B-cell response*. Immunology, 2009. **128**(3): p. 311-23.
13. Meyer-Bahlburg, A. and D.J. Rawlings, *B cell autonomous TLR signaling and autoimmunity*. Autoimmun Rev, 2008. **7**(4): p. 313-6.
14. Racine, R. and G.M. Winslow, *IgM in microbial infections: taken for granted?* Immunol Lett, 2009. **125**(2): p. 79-85.
15. Hayakawa, K., et al., *The "Ly-1 B" cell subpopulation in normal immunodefective, and autoimmune mice*. J Exp Med, 1983. **157**(1): p. 202-18.
16. Montecino-Rodriguez, E. and K. Dorshkind, *B-1 B cell development in the fetus and adult*. Immunity, 2012. **36**(1): p. 13-21.
17. Cerutti, A., M. Cols, and I. Puga, *Marginal zone B cells: virtues of innate-like antibody-producing lymphocytes*. Nat Rev Immunol, 2013. **13**(2): p. 118-32.
18. Kaminski, D.A. and J. Stavnezer, *Enhanced IgA class switching in marginal zone and B1 B cells relative to follicular/B2 B cells*. J Immunol, 2006. **177**(9): p. 6025-9.
19. Yoshimoto, M., et al., *Embryonic day 9 yolk sac and intra-embryonic hemogenic endothelium independently generate a B-1 and marginal zone progenitor lacking B-2 potential*. Proc Natl Acad Sci U S A, 2011. **108**(4): p. 1468-73.
20. Casola, S., et al., *B cell receptor signal strength determines B cell fate*. Nat Immunol, 2004. **5**(3): p. 317-27.
21. Martin, F., A.M. Oliver, and J.F. Kearney, *Marginal zone and B1 B cells unite in the early response against T-independent blood-borne particulate antigens*. Immunity, 2001. **14**(5): p. 617-29.
22. Song, H. and J. Cerny, *Functional heterogeneity of marginal zone B cells revealed by their ability to generate both early antibody-forming cells and germinal centers with hypermutation and memory in response to a T-dependent antigen*. J Exp Med, 2003. **198**(12): p. 1923-35.
23. Genestier, L., et al., *TLR agonists selectively promote terminal plasma cell differentiation of B cell subsets specialized in thymus-independent responses*. J Immunol, 2007. **178**(12): p. 7779-86.

24. Itoh, K., et al., *Clonal expansion is a characteristic feature of the B-cell repetoire of patients with rheumatoid arthritis*. Arthritis Res, 2000. **2**(1): p. 50-8.
25. Vinh, A., et al., *Inhibition and genetic ablation of the B7/CD28 T-cell costimulation axis prevents experimental hypertension*. Circulation, 2010. **122**(24): p. 2529-37.
26. Figueiredo Galvao, H.B., et al., *Proteasome inhibition reduces plasma cell and antibody secretion, but not angiotensin II-induced hypertension*. Front Cardiovasc Med, 2023. **10**: p. 1184982.
27. Monaco, G., et al., *flowAI: automatic and interactive anomaly discerning tools for flow cytometry data*. Bioinformatics, 2016. **32**(16): p. 2473-80.
28. Pedersen, C.B., et al., *cyCombine allows for robust integration of single-cell cytometry datasets within and across technologies*. Nat Commun, 2022. **13**(1): p. 1698.
29. Finak G, J.M., *flowWorkspace: Infrastructure for representing and interacting with gated and ungated cytometry data sets*. 2024.
30. Stall, A.M., et al., *Characteristics and development of the murine B-1b (Ly-1 B sister) cell population*. Ann N Y Acad Sci, 1992. **651**: p. 33-43.
31. Butler, A., et al., *Integrating single-cell transcriptomic data across different conditions, technologies, and species*. Nat Biotechnol, 2018. **36**(5): p. 411-420.
32. Hao, Y., et al., *Integrated analysis of multimodal single-cell data*. Cell, 2021. **184**(13): p. 3573-3587 e29.
33. Satija, R., et al., *Spatial reconstruction of single-cell gene expression data*. Nat Biotechnol, 2015. **33**(5): p. 495-502.
34. McGinnis, C.S., L.M. Murrow, and Z.J. Gartner, *DoubletFinder: Doublet Detection in Single-Cell RNA Sequencing Data Using Artificial Nearest Neighbors*. Cell Syst, 2019. **8**(4): p. 329-337 e4.
35. Traag, V.A., L. Waltman, and N.J. van Eck, *From Louvain to Leiden: guaranteeing well-connected communities*. Sci Rep, 2019. **9**(1): p. 5233.
36. Cao, J., et al., *The single-cell transcriptional landscape of mammalian organogenesis*. Nature, 2019. **566**(7745): p. 496-502.
37. Qiu, X., et al., *Reversed graph embedding resolves complex single-cell trajectories*. Nat Methods, 2017. **14**(10): p. 979-982.
38. Trapnell, C., et al., *The dynamics and regulators of cell fate decisions are revealed by pseudotemporal ordering of single cells*. Nat Biotechnol, 2014. **32**(4): p. 381-386.
39. Aran, D., et al., *Reference-based analysis of lung single-cell sequencing reveals a transitional profibrotic macrophage*. Nat Immunol, 2019. **20**(2): p. 163-172.
40. Liberzon, A., et al., *The Molecular Signatures Database (MSigDB) hallmark gene set collection*. Cell Syst, 2015. **1**(6): p. 417-425.
41. Subramanian, A., et al., *Gene set enrichment analysis: a knowledge-based approach for interpreting genome-wide expression profiles*. Proc Natl Acad Sci U S A, 2005. **102**(43): p. 15545-50.
42. Wu, T., et al., *clusterProfiler 4.0: A universal enrichment tool for interpreting omics data*. Innovation (Camb), 2021. **2**(3): p. 100141.
43. Yu, G., et al., *clusterProfiler: an R package for comparing biological themes among gene clusters*. OMICS, 2012. **16**(5): p. 284-7.
44. Wickham, H., *ggplot2: Elegant Graphics for Data Analysis*. 2016: Springer-Verlag New York.

45. Yaari, G. and S.H. Kleinstein, *Practical guidelines for B-cell receptor repertoire sequencing analysis*. Genome Med, 2015. **7**: p. 121.
46. Merkel, D., *Docker: lightweight linux containers for consistent development and deployment*. Linux Journal, 2014. **2014**(239): p. 2.
47. Wong, W.K., J. Leem, and C.M. Deane, *Comparative Analysis of the CDR Loops of Antigen Receptors*. Front Immunol, 2019. **10**: p. 2454.
48. Nouri, N. and S.H. Kleinstein, *Somatic hypermutation analysis for improved identification of B cell clonal families from next-generation sequencing data*. PLoS Comput Biol, 2020. **16**(6): p. e1007977.
49. Nouri, N. and S.H. Kleinstein, *A spectral clustering-based method for identifying clones from high-throughput B cell repertoire sequencing data*. Bioinformatics, 2018. **34**(13): p. i341-i349.
50. Gupta, N.T., et al., *Change-O: a toolkit for analyzing large-scale B cell immunoglobulin repertoire sequencing data*. Bioinformatics, 2015. **31**(20): p. 3356-8.
51. Borcherding, N., N.L. Bormann, and G. Kraus, *scRepertoire: An R-based toolkit for single-cell immune receptor analysis*. F1000Res, 2020. **9**: p. 47.
52. Lee, R.D., et al., *Single-cell analysis identifies dynamic gene expression networks that govern B cell development and transformation*. Nat Commun, 2021. **12**(1): p. 6843.
53. Hagman, J., A. Travis, and R. Grosschedl, *A novel lineage-specific nuclear factor regulates mb-1 gene transcription at the early stages of B cell differentiation*. EMBO J, 1991. **10**(11): p. 3409-17.
54. Sigvardsson, M., et al., *Early B-cell factor, E2A, and Pax-5 cooperate to activate the early B cell-specific mb-1 promoter*. Mol Cell Biol, 2002. **22**(24): p. 8539-51.
55. Akerblad, P., et al., *The B29 (immunoglobulin beta-chain) gene is a genetic target for early B-cell factor*. Mol Cell Biol, 1999. **19**(1): p. 392-401.
56. Inlay, M.A., et al., *Ly6d marks the earliest stage of B-cell specification and identifies the branchpoint between B-cell and T-cell development*. Genes Dev, 2009. **23**(20): p. 2376-81.
57. Li, R., et al., *Dynamic EBF1 occupancy directs sequential epigenetic and transcriptional events in B-cell programming*. Genes Dev, 2018. **32**(2): p. 96-111.
58. Mason, D.Y., et al., *CD79a: a novel marker for B-cell neoplasms in routinely processed tissue samples*. Blood, 1995. **86**(4): p. 1453-9.
59. Tedder, T.F., *CD19: a promising B cell target for rheumatoid arthritis*. Nat Rev Rheumatol, 2009. **5**(10): p. 572-7.
60. Hardy, R.R., et al., *Resolution and characterization of pro-B and pre-pro-B cell stages in normal mouse bone marrow*. J Exp Med, 1991. **173**(5): p. 1213-25.
61. Li, Y.S., K. Hayakawa, and R.R. Hardy, *The regulated expression of B lineage associated genes during B cell differentiation in bone marrow and fetal liver*. J Exp Med, 1993. **178**(3): p. 951-60.
62. Karasuyama, H., A. Rolink, and F. Melchers, *Surrogate light chain in B cell development*. Adv Immunol, 1996. **63**: p. 1-41.
63. Liu, X., et al., *PCLAF promotes neuroblastoma G1/S cell cycle progression via the E2F1/PTTG1 axis*. Cell Death Dis, 2022. **13**(2): p. 178.

64. Ramamoorthy, M., et al., *RECQL5 cooperates with Topoisomerase II alpha in DNA decatenation and cell cycle progression*. Nucleic Acids Res, 2012. **40**(4): p. 1621-35.
65. Reth, M., et al., *Activation of V kappa gene rearrangement in pre-B cells follows the expression of membrane-bound immunoglobulin heavy chains*. EMBO J, 1987. **6**(11): p. 3299-305.
66. Schlissel, M.S. and D. Baltimore, *Activation of immunoglobulin kappa gene rearrangement correlates with induction of germline kappa gene transcription*. Cell, 1989. **58**(5): p. 1001-7.
67. Mandal, M., et al., *Epigenetic repression of the Igk locus by STAT5-mediated recruitment of the histone methyltransferase Ezh2*. Nat Immunol, 2011. **12**(12): p. 1212-20.
68. Clark, M.R., et al., *Orchestrating B cell lymphopoiesis through interplay of IL-7 receptor and pre-B cell receptor signalling*. Nat Rev Immunol, 2014. **14**(2): p. 69-80.
69. Henderson, R.B., et al., *A novel Rac-dependent checkpoint in B cell development controls entry into the splenic white pulp and cell survival*. J Exp Med, 2010. **207**(4): p. 837-53.
70. Petro, J.B., et al., *Transitional type 1 and 2 B lymphocyte subsets are differentially responsive to antigen receptor signaling*. J Biol Chem, 2002. **277**(50): p. 48009-19.
71. Schiemann, B., et al., *An essential role for BAFF in the normal development of B cells through a BCMA-independent pathway*. Science, 2001. **293**(5537): p. 2111-4.
72. Sasaki, Y., et al., *TNF family member B cell-activating factor (BAFF) receptor-dependent and -independent roles for BAFF in B cell physiology*. J Immunol, 2004. **173**(4): p. 2245-52.
73. Newman, R., et al., *Maintenance of the marginal-zone B cell compartment specifically requires the RNA-binding protein ZFP36L1*. Nat Immunol, 2017. **18**(6): p. 683-693.
74. Andreani, V., et al., *Cochaperone Mzb1 is a key effector of Blimp1 in plasma cell differentiation and beta1-integrin function*. Proc Natl Acad Sci U S A, 2018. **115**(41): p. E9630-E9639.
75. Dominguez, P.M. and R. Shaknovich, *Epigenetic function of activation-induced cytidine deaminase and its link to lymphomagenesis*. Front Immunol, 2014. **5**: p. 642.
76. Laidlaw, B.J. and J.G. Cyster, *Transcriptional regulation of memory B cell differentiation*. Nat Rev Immunol, 2021. **21**(4): p. 209-220.
77. Yang, L., et al., *DOCK2 couples with LEF-1 to regulate B cell metabolism and memory response*. Biochem Biophys Res Commun, 2020. **529**(2): p. 296-302.
78. Tay, C., et al., *Follicular B Cells Promote Atherosclerosis via T Cell-Mediated Differentiation Into Plasma Cells and Secreting Pathogenic Immunoglobulin G*. Arterioscler Thromb Vasc Biol, 2018. **38**(5): p. e71-e84.
79. Scharer, C.D., et al., *Plasma cell differentiation is controlled by multiple cell division-coupled epigenetic programs*. Nat Commun, 2018. **9**(1): p. 1698.
80. Scharer, C.D., et al., *Antibody-secreting cell destiny emerges during the initial stages of B-cell activation*. Nat Commun, 2020. **11**(1): p. 3989.

81. Ning, S., J.S. Pagano, and G.N. Barber, *IRF7: activation, regulation, modification and function*. Genes Immun, 2011. **12**(6): p. 399-414.
82. Naranjo, N.M., et al., *IFIT3 (interferon induced protein with tetratricopeptide repeats 3) modulates STAT1 expression in small extracellular vesicles*. Biochem J, 2021. **478**(21): p. 3905-3921.
83. Wardlaw, C.P. and J.H.J. Petrini, *ISG15: A link between innate immune signaling, DNA replication, and genome stability*. Bioessays, 2023: p. e2300042.
84. Kim, G.S., et al., *Single-cell analysis identifies Ifi27l2a as a novel gene regulator of microglial inflammation in the context of aging and stroke*. Res Sq, 2023.
85. Sooreshjani, M.A., et al., *Proteomic analysis of RAW macrophages treated with cGAMP or c-di-GMP reveals differentially activated cellular pathways*. RSC Adv, 2018. **8**(64): p. 36840-36851.
86. Lee, H.R., et al., *Viral interferon regulatory factors*. J Interferon Cytokine Res, 2009. **29**(9): p. 621-7.
87. Iwakoshi, N.N., et al., *Plasma cell differentiation and the unfolded protein response intersect at the transcription factor XBP-1*. Nat Immunol, 2003. **4**(4): p. 321-9.
88. Segundo, C., et al., *Thyroid-infiltrating B lymphocytes in Graves' disease are related to marginal zone and memory B cell compartments*. Thyroid, 2001. **11**(6): p. 525-30.
89. Marino, E., et al., *Marginal-zone B-cells of nonobese diabetic mice expand with diabetes onset, invade the pancreatic lymph nodes, and present autoantigen to diabetogenic T-cells*. Diabetes, 2008. **57**(2): p. 395-404.
90. Wither, J.E., A.D. Paterson, and B. Vukusic, *Genetic dissection of B cell traits in New Zealand black mice. The expanded population of B cells expressing up-regulated costimulatory molecules shows linkage to Nba2*. Eur J Immunol, 2000. **30**(2): p. 356-65.
91. Dinh, Q.N., et al., *Aldosterone-induced hypertension is sex-dependent, mediated by T cells and sensitive to GPER activation*. Cardiovasc Res, 2021. **117**(3): p. 960-970.
92. Pollow, D.P., Jr., et al., *ANG II-induced hypertension in the VCD mouse model of menopause is prevented by estrogen replacement during perimenopause*. Am J Physiol Regul Integr Comp Physiol, 2015. **309**(12): p. R1546-52.
93. Sender, R., et al., *The total mass, number, and distribution of immune cells in the human body*. Proc Natl Acad Sci U S A, 2023. **120**(44): p. e2308511120.
94. Billi, A.C., J.M. Kahlenberg, and J.E. Gudjonsson, *Sex bias in autoimmunity*. Curr Opin Rheumatol, 2019. **31**(1): p. 53-61.
95. Mizoguchi, A., et al., *Chronic intestinal inflammatory condition generates IL-10-producing regulatory B cell subset characterized by CD1d upregulation*. Immunity, 2002. **16**(2): p. 219-30.
96. Fillatreau, S., et al., *B cells regulate autoimmunity by provision of IL-10*. Nat Immunol, 2002. **3**(10): p. 944-50.
97. Mauri, C., et al., *Prevention of arthritis by interleukin 10-producing B cells*. J Exp Med, 2003. **197**(4): p. 489-501.
98. Snapper, C.M., et al., *Comparative in vitro analysis of proliferation, Ig secretion, and Ig class switching by murine marginal zone and follicular B cells*. J Immunol, 1993. **150**(7): p. 2737-45.

99. Snapper, C.M. and W.E. Paul, *Interferon-gamma and B cell stimulatory factor-1 reciprocally regulate Ig isotype production*. Science, 1987. **236**(4804): p. 944-7.
100. Cerutti, A., *The regulation of IgA class switching*. Nat Rev Immunol, 2008. **8**(6): p. 421-34.
101. Figueiredo Galvao, H.B., et al., *Depletion of follicular B cell-derived antibody secreting cells does not attenuate angiotensin II-induced hypertension or vascular compliance*. Front Cardiovasc Med, 2024. **11**: p. 1419958.
102. Cinamon, G., et al., *Follicular shuttling of marginal zone B cells facilitates antigen transport*. Nat Immunol, 2008. **9**(1): p. 54-62.
103. Cinamon, G., et al., *Sphingosine 1-phosphate receptor 1 promotes B cell localization in the splenic marginal zone*. Nat Immunol, 2004. **5**(7): p. 713-20.
104. Spencer, J., et al., *The human gut contains a novel population of B lymphocytes which resemble marginal zone cells*. Clin Exp Immunol, 1985. **62**(3): p. 607-12.
105. Tierens, A., et al., *Marginal-zone B cells in the human lymph node and spleen show somatic hypermutations and display clonal expansion*. Blood, 1999. **93**(1): p. 226-34.
106. Dono, M., et al., *Heterogeneity of tonsillar subepithelial B lymphocytes, the splenic marginal zone equivalents*. J Immunol, 2000. **164**(11): p. 5596-604.
107. Cariappa, A., et al., *Perisinusoidal B cells in the bone marrow participate in T-independent responses to blood-borne microbes*. Immunity, 2005. **23**(4): p. 397-407.
108. Zhu, F., et al., *Correlation between HLA-DRB1, HLA-DQB1 polymorphism and autoantibodies against angiotensin AT(1) receptors in Chinese patients with essential hypertension*. Clin Cardiol, 2011. **34**(5): p. 302-8.
109. Liao, Y.H., et al., *Autoantibodies against AT1-receptor and alpha1-adrenergic receptor in patients with hypertension*. Hypertens Res, 2002. **25**(4): p. 641-6.
110. Fu, M.L., et al., *Autoantibodies against the angiotensin receptor (AT1) in patients with hypertension*. J Hypertens, 2000. **18**(7): p. 945-53.
111. LaMarca, B., et al., *Hypertension in response to autoantibodies to the angiotensin II type I receptor (AT1-AA) in pregnant rats: role of endothelin-1*. Hypertension, 2009. **54**(4): p. 905-9.
112. Tay, C., et al., *B-cell-specific depletion of tumour necrosis factor alpha inhibits atherosclerosis development and plaque vulnerability to rupture by reducing cell death and inflammation*. Cardiovasc Res, 2016. **111**(4): p. 385-97.
113. Barr, T.A., et al., *B cell depletion therapy ameliorates autoimmune disease through ablation of IL-6-producing B cells*. J Exp Med, 2012. **209**(5): p. 1001-10.
114. Olalekan, S.A., et al., *B cells expressing IFN-gamma suppress Treg-cell differentiation and promote autoimmune experimental arthritis*. Eur J Immunol, 2015. **45**(4): p. 988-98.
115. Ashouri, J.F. and A. Weiss, *Endogenous Nur77 Is a Specific Indicator of Antigen Receptor Signaling in Human T and B Cells*. J Immunol, 2017. **198**(2): p. 657-668.
116. Jumper, J., et al., *Highly accurate protein structure prediction with AlphaFold*. Nature, 2021. **596**(7873): p. 583-589.
117. Ruffolo, J.A., et al., *Fast, accurate antibody structure prediction from deep learning on massive set of natural antibodies*. Nat Commun, 2023. **14**(1): p. 2389.
118. Ponnuswamy, P., et al., *Angiotensin II synergizes with BAFF to promote atheroprotective regulatory B cells*. Sci Rep, 2017. **7**(1): p. 4111.

Figure legends

Figure 1: Earliest committed progenitor B cells through to terminally differentiated plasma cells were captured in the spleen and bone marrow by single cell transcriptomics. Early-stage B cell markers (a), proliferative and transitional B cell markers (b) and mature B cell markers (c) shown in violin plots. d) Top 5 uniquely expressed genes for each population where the size and colour of each dot represents the percentage of cells expressing a given gene in that cluster and its normalized expression count, respectively. Immature B cell populations found exclusively in the bone marrow are shown in cornflower blue. Pre-BCRd = pre-B cell receptor dependent cells; Pre-BCRi = pre-B cell receptor independent cells; Tr1 = transitional B cells found in bone marrow; Tr2 = transitional B cells found in spleen; MZB = marginal zone B cells; Bmem = memory B cells; GC = germinal center B cells; PCs = plasma cells; Circ. B-2 = circulating B-2 cells.

Figure 2: Pseudotime trajectory projection and gene ontology modules corroborate with identified B cell subtypes. a) Three-dimensional (3D) pseudotime trajectory (black trace with arrows) showing the maturation of B cells from the bone marrow to the spleen. Genes expressed in specific regions of the 3D space were grouped into modules, visualised using a heatmap (b) and gene ontologies were obtained to identify cell functions (panels c and d). In panels ‘c’ and ‘d’, the size and colour of each dot represents the number of genes expressed in a given gene ontology and its q value, respectively. Pre-BCRd = pre-B cell receptor dependent cells; Pre-BCRi = pre-B cell receptor independent cells; Tr1 = transitional B cells found in bone marrow; Tr2 = transitional B cells found in spleen; MZB = marginal zone B cells; Bmem = memory B cells; GC = germinal center B cells; PCs = plasma cells; Circ. B-2 = circulating B-2 cells.

Figure 3: Expansion and activation of marginal zone B cells in hypertensive mice. Systolic blood pressures (a) in vehicle (0.5% NaCl, 0.1% acetic acid) and angiotensin II (0.70 mg/kg/day)-infused mice. b) UMAP dimensional reduction of B cells from normotensive and

hypertensive mice split by treatment. c) Bar graph highlighting in ochre the percentage of marginal zone B cells (MZB) for each treatment group. Bar graph and corresponding plots of flow cytometry data showing an increase in $CD21^{hi}CD23^{neg}$ MZB (d), as well as an increase in non-specific B cell activation (CD69; e) and B cell receptor (BCR)-specific B cell activation (Nur77; f), as a percentage of all live spleen cells. For a), d), e) and f) data are represented as the mean ± standard error of the mean. Systolic blood pressures were analysed using a two-way ANOVA. **** indicates a P value <0.0001. Treatment effects are indicated by P_{ANG} for angiotensin II, P_{DAYS} for time, and $P_{DAYS*ANG}$ for interaction effects. Flow cytometry data was analysed using a two-tailed unpaired student's T test. P values are indicated above bar graphs. Immature B cell populations found exclusively in the bone marrow are shown in cornflower blue. Pre-BCRd = pre-B cell receptor dependent cells; Pre-BCRi = pre-B cell receptor independent cells; Tr1 = transitional B cells found in bone marrow; Tr2 = transitional B cells found in spleen; MZB = marginal zone B cells; Bmem = memory B cells; GC = germinal center B cells; PCs = plasma cells; Circ. B-2 = circulating B-2 cells.

Figure 4: Marginal zone-like B cells infiltrate the kidneys of hypertensive mice, are activated and form memory B cells. Bar graphs and corresponding plots of flow cytometry data showing infiltration of B cells, including MZB-like cells, non-specific MZB-like activation (CD69), B cell receptor-specific MZB-like activation (Nur77) and MZB-like memory B cells (CD27) in panels a-e, respectively, in kidneys from normotensive and hypertensive mice. MZB-like cells were identified as $CD19^{+}CD24^{neg}B220^{+}CD21^{+}CD23^{neg}$ live cells. Data are represented as the mean ± standard error of the mean. Flow cytometry data was analysed using a two-tailed unpaired student's T test, with P values shown above bar graphs.

Figure 5: Reduced B cell receptor (BCR) diversity, BCR clonal expansion and increased expression of IGHV1 BCR variants in hypertension. Plots showing total BCR diversity (a) and IgM-only BCR diversity (b) in vehicle (normotensive) and angiotensin II-infused (hypertensive) mice. Hill numbers (q) were used to calculate diversity (qD) metrics of BCR

samples. Hill numbers can be interpreted over intervals where q = 0 represents species richness, q = 1 the Shannon Entropy of a population and q = 2 the Simpson Index, where Shannon and Simpson indices reflect species diversity. Within diversity curves, the darker solid line and its corresponding lighter band represents the mean and 95% confidence intervals, respectively. Lower qD values indicate reduced diversity and bands which do not overlap are statistically significant. c) Bar graph showing the number of expanded B cell clones in sequenced spleens. d) Venn diagram showing number of overlapping clones in normotensive and hypertensive mice. e) Plots showing mean effect size changes of treatment effects (VEH:ANG II) on the frequency of variable gene segments in antibody heavy and light chains from the spleen. For c) data are represented as the mean ± standard error of the mean, where data was analysed using a two-tailed unpaired student's T test. For e) hypothesis testing was performed using a two-way ANOVA. MZB = marginal zone B cells.

Figure 6: Female mice have a slower response to angiotensin II and lower cardiac hypertrophy but no difference in marginal zone B cell expansion. Systolic blood pressures (a) of vehicle (0.5% NaCl, 0.1% acetic acid) and angiotensin II (0.70 mg/kg/day)-infused male and female mice. Heart-weight to tibia length ratios of male and female normotensive and hypertensive mice (b). c) Table summarizing flow cytometry data from marginal zone B cell populations of normotensive and hypertensive male and female mice. Marginal zone B cells (MZB) and MZB-like cells were identified as $CD19^{+}CD24^{neg}$ $B220^{+}CD21^{+}CD23^{neg}$ B cells as a percentage of live cells. In all figures and table, data are represented as the mean ± standard error of the mean. Flow cytometry data was analysed using a two-way ANOVA while systolic blood pressures were analysed using a three-way ANOVA. Treatment effects are indicated by P_{ANG} for angiotensin II, P_{SEX} for sex-specific effects, $P_{SEX*ANG}$ and $P_{DAYS*SEX*ANG}$ for interaction effects.

Figure 7: Genetic depletion of MZBs blunts angiotensin II-induced hypertension. Bar graphs and corresponding plots of flow cytometry data showing the percentage of live marginal

zone B cells (MZB) ($CD19^{+}CD24^{neg}B220^{+}CD21^{+}CD23^{neg}$) in the spleens of vehicle (0.5% NaCl, 0.1% acetic acid) and angiotensin II (0.70 mg/kg/day)-infused male C57 and BAFF-R knock out mice (a). Systolic blood pressures (b) in normotensive (vehicle-infused) and hypertensive (angiotensin II-infused) mice. Data are represented as the mean ± standard error of the mean. Flow cytometry data was analysed using a two-way ANOVA with P values shown above bar graphs. Systolic blood pressures were analysed using a three-way ANOVA. Treatment effects are indicated by P_{ANG} for angiotensin II and $P_{GENOTYPE}$ for genotypes.

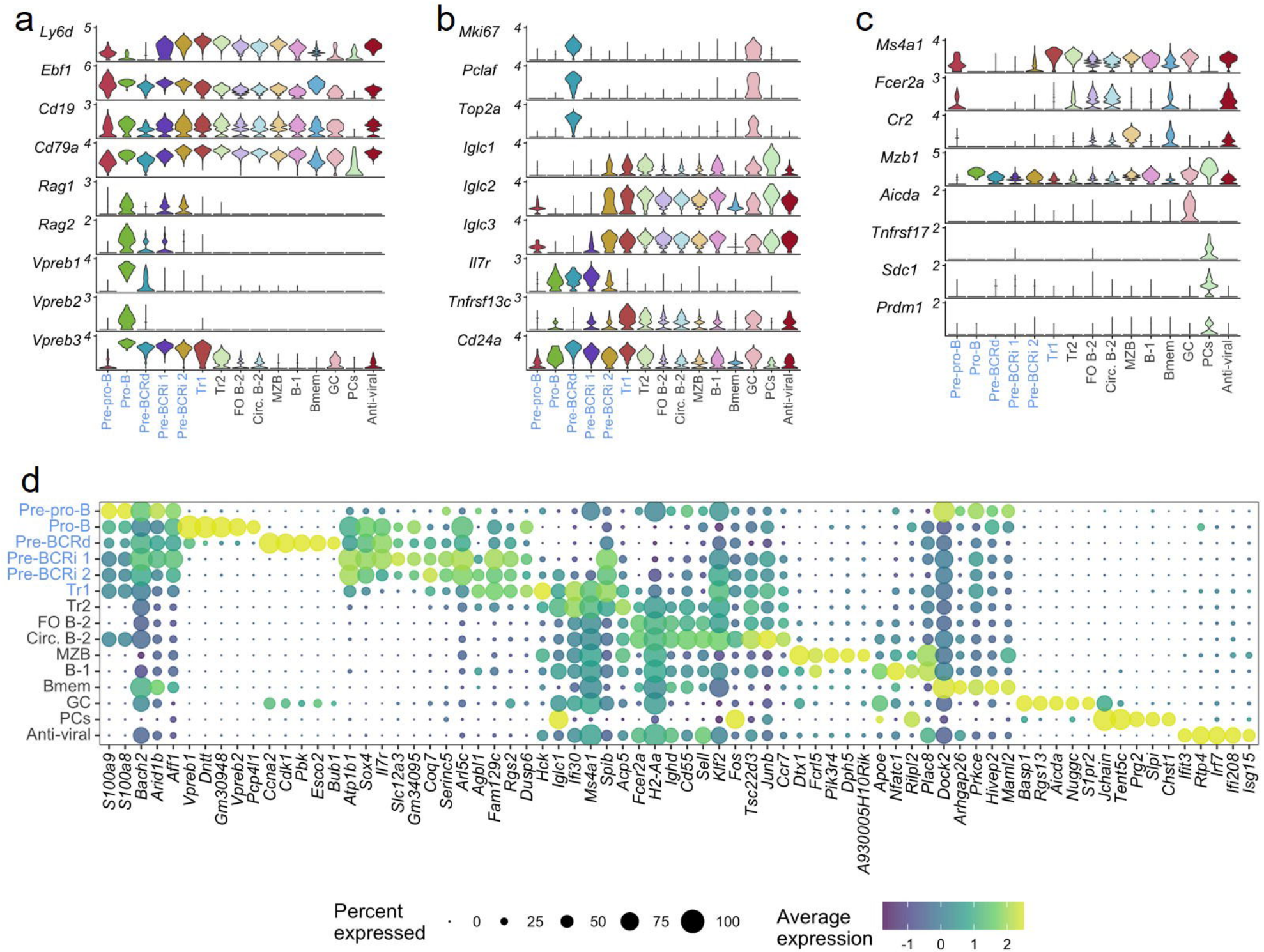
a
Ly6d
Ebf1
Cd19
Cd79a
Rag1
Rag2
Vpreb1
Vpreb2
Vpreb3
b
Mki67
Pclaf
Top2a
Iglc1
Iglc2
Iglc3
Il7r
Tnfrsf13c
Cd24a
c
Ms4a1
Fcer2a
Cr2
Mzb1
Aicda
Tnfrsf17
Sdc1
Prdm1
Pre-pro-B
Pro-B
Pre-BCRd
Pre-BCRi 1
Pre-BCRi 2
Tr1
Tr2
FO B-2
Circ. B-2
MZB
B-1
Bmem
GC
PCs
Anti-viral
d
S100a9
S100a8
Bach2
Arid1b
Aff1
Vpreb1
Dntt
Gm30948
Vpreb2
Pcp4l1
Ccna2
Cdk1
Pbk
Esco2
Bub1
Atp1b1
Sox4
Il7r
Slc12a3
Gm34095
Coq7
Serinc5
Arl5c
Agbl1
Fam129c
Rgs2
Dusp6
Hck
Iglc1
Ifi30
Ms4a1
Spib
Acp5
Fcer2a
H2-Aa
Ighd
Cd55
Sell
Klf2
Fos
Tsc22d3
Junb
Ccr7
Dtx1
Fcrl5
Pik3r4
Dph5
A930005H10Rik
Apoe
Nfatc1
Rilpl2
Plac8
Dock2
Arhgap26
Prkce
Hivep2
Maml2
Basp1
Rgs13
Aicda
Nuggc
S1pr2
Jchain
Tent5c
Prg2
Slpi
Chst1
Ifit3
Rtp4
Irf7
Ifi208
Isg15
Percent expressed
0
25
50
75
100
Average expression
-1
0
1
2

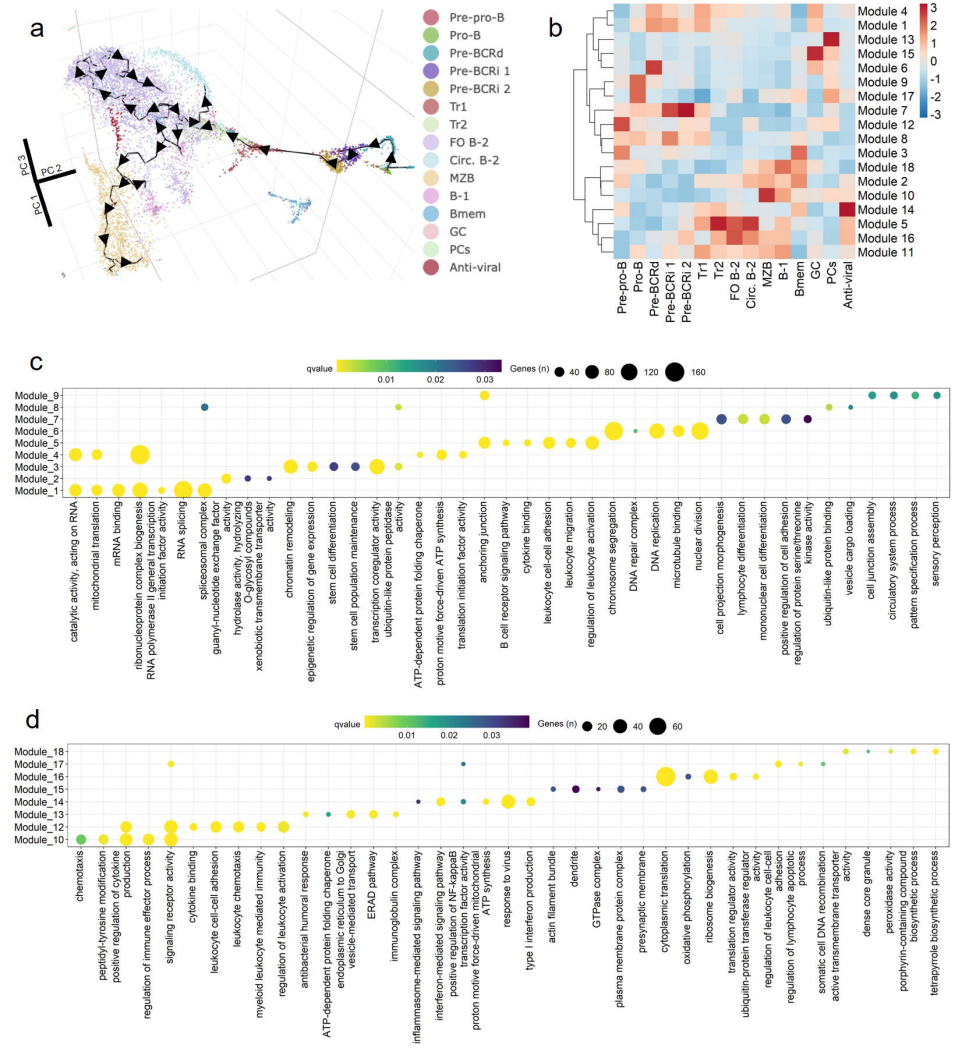
a
PC 1
PC 2
PC 3
Pre-pro-B
Pro-B
Pre-BCRd
Pre-BCRi 1
Pre-BCRi 2
Tr1
Tr2
FO B-2
Circ. B-2
MZB
B-1
Bmem
GC
PCs
Anti-viral
b
Module 4
Module 1
Module 13
Module 15
Module 6
Module 9
Module 17
Module 7
Module 12
Module 8
Module 3
Module 18
Module 2
Module 10
Module 14
Module 5
Module 16
Module 11
3
2
1
0
-1
-2
-3
c
qvalue
0.01
0.02
0.03
Genes (n)
40
80
120
160
Module_9
Module_8
Module_7
Module_6
Module_5
Module_4
Module_3
Module_2
Module_1
catalytic activity, acting on RNA
mitochondrial translation
mRNA binding
ribonucleoprotein complex biogenesis
RNA polymerase II general transcription initiation factor activity
RNA splicing
spliceosomal complex
guanyl-nucleotide exchange factor activity
hydrolase activity, hydrolyzing O-glycosyl compounds
xenobiotic transmembrane transporter activity
chromatin remodeling
epigenetic regulation of gene expression
stem cell differentiation
stem cell population maintenance
transcription coregulator activity
ubiquitin-like protein peptidase activity
ATP-dependent protein folding chaperone
proton motive force-driven ATP synthesis
translation initiation factor activity
anchoring junction
B cell receptor signaling pathway
cytokine binding
leukocyte cell-cell adhesion
leukocyte migration
regulation of leukocyte activation
chromosome segregation
DNA repair complex
DNA replication
microtubule binding
nuclear division
cell projection morphogenesis
lymphocyte differentiation
mononuclear cell differentiation
positive regulation of cell adhesion
regulation of protein serine/threonine kinase activity
ubiquitin-like protein binding
vesicle cargo loading
cell junction assembly
circulatory system process
pattern specification process
sensory perception
d
qvalue
0.01
0.02
0.03
Genes (n)
20
40
60
Module_18
Module_17
Module_16
Module_15
Module_14
Module_13
Module_12
Module_10
chemotaxis
peptidyl-tyrosine modification
positive regulation of cytokine production
regulation of immune effector process
signaling receptor activity
cytokine binding
leukocyte cell-cell adhesion
leukocyte chemotaxis
myeloid leukocyte mediated immunity
regulation of leukocyte activation
antibacterial humoral response
ATP-dependent protein folding chaperone
endoplasmic reticulum to Golgi vesicle-mediated transport
ERAD pathway
immunoglobulin complex
inflammasome-mediated signaling pathway
interferon-mediated signaling pathway
positive regulation of NF-kappaB transcription factor activity
proton motive force-driven mitochondrial ATP synthesis
response to virus
type I interferon production
actin filament bundle
dendrite
GTPase complex
plasma membrane protein complex
presynaptic membrane
cytoplasmic translation
oxidative phosphorylation
ribosome biogenesis
translation regulator activity
ubiquitin-protein transferase regulator activity
regulation of leukocyte cell-cell adhesion
regulation of lymphocyte apoptotic process
somatic cell DNA recombination
active transmembrane transporter activity
dense core granule
peroxidase activity
porphyrin-containing compound biosynthetic process
tetrapyrrole biosynthetic process

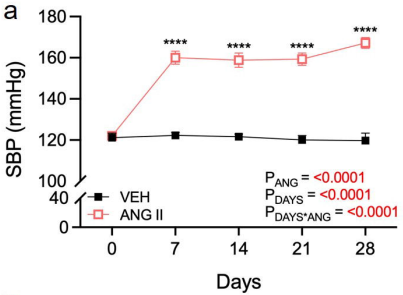
a
SBP (mmHg)
180
160
140
120
100
40
0
****
VEH
ANG II
P_{ANG} = <0.0001
P_{DAYS} = <0.0001
$P_{DAYS*ANG}$ = <0.0001
0
7
14
21
28
Days

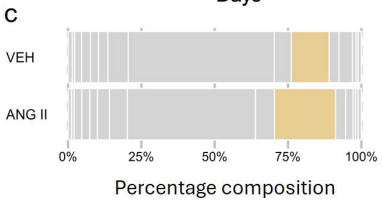
c
VEH
ANG II
0%
25%
50%
75%
100%
Percentage composition

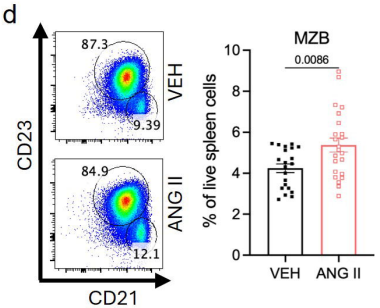
d
CD23
CD21
87.3
9.39
84.9
12.1
VEH
ANG II
MZB
0.0086
% of live spleen cells
VEH
ANG II

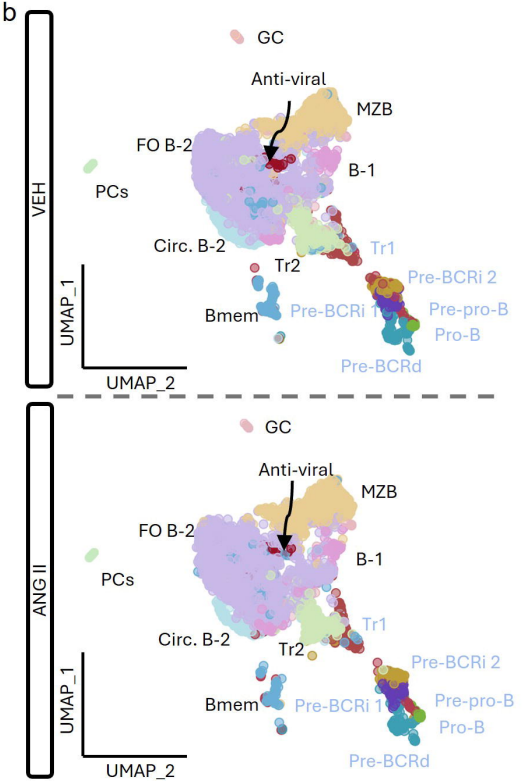
b
VEH
ANG II
GC
Anti-viral
MZB
FO B-2
B-1
PCs
Circ. B-2
Tr1
Tr2
Pre-BCRi 2
Bmem
Pre-BCRi 1
Pre-pro-B
Pro-B
Pre-BCRd
UMAP_1
UMAP_2

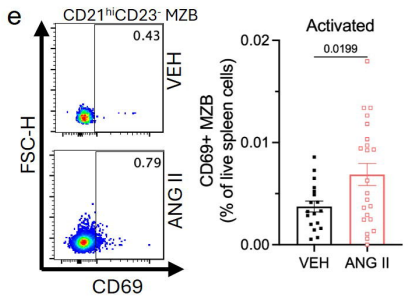
e
CD21hiCD23- MZB
FSC-H
CD69
0.43
0.79
VEH
ANG II
Activated
0.0199
CD69+ MZB
(% of live spleen cells)
VEH
ANG II

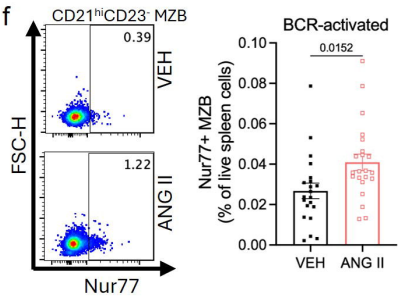
f
CD21hiCD23- MZB
FSC-H
Nur77
0.39
1.22
VEH
ANG II
BCR-activated
0.0152
Nur77+ MZB
(% of live spleen cells)
VEH
ANG II

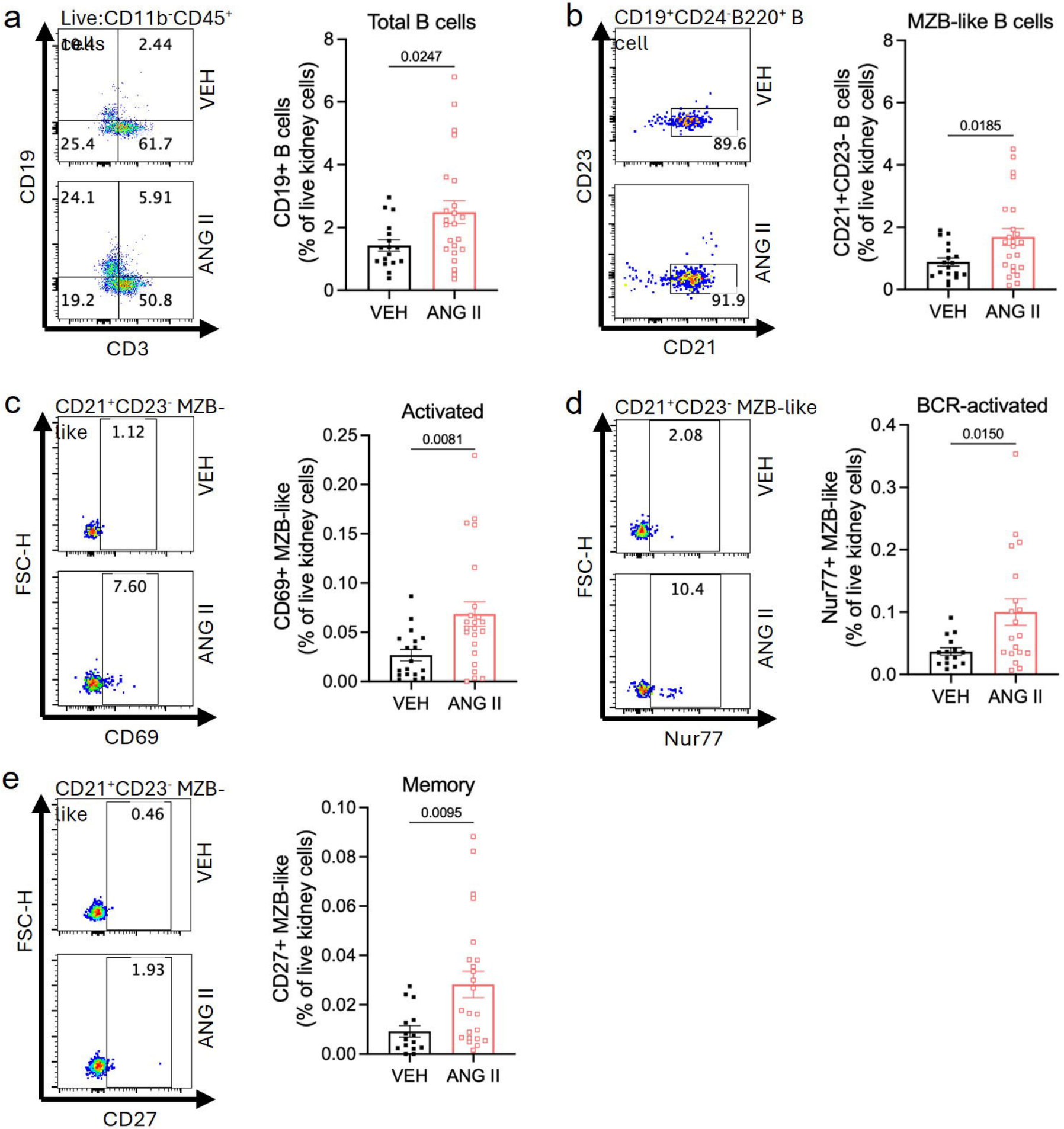
a
Live:CD11b-CD45+ cells
2.44
25.4
61.7
VEH
24.1
5.91
19.2
50.8
ANG II
CD19
CD3
Total B cells
0.0247
CD19+ B cells (% of live kidney cells)
VEH
ANG II
b
CD19+CD24-B220+ B cell
89.6
VEH
91.9
ANG II
CD23
CD21
MZB-like B cells
0.0185
CD21+CD23- B cells (% of live kidney cells)
VEH
ANG II
c
CD21+CD23- MZB-like
1.12
VEH
7.60
ANG II
FSC-H
CD69
Activated
0.0081
CD69+ MZB-like (% of live kidney cells)
VEH
ANG II
d
CD21+CD23- MZB-like
2.08
VEH
10.4
ANG II
FSC-H
Nur77
BCR-activated
0.0150
Nur77+ MZB-like (% of live kidney cells)
VEH
ANG II
e
CD21+CD23- MZB-like
0.46
VEH
1.93
ANG II
FSC-H
CD27
Memory
0.0095
CD27+ MZB-like (% of live kidney cells)
VEH
ANG II

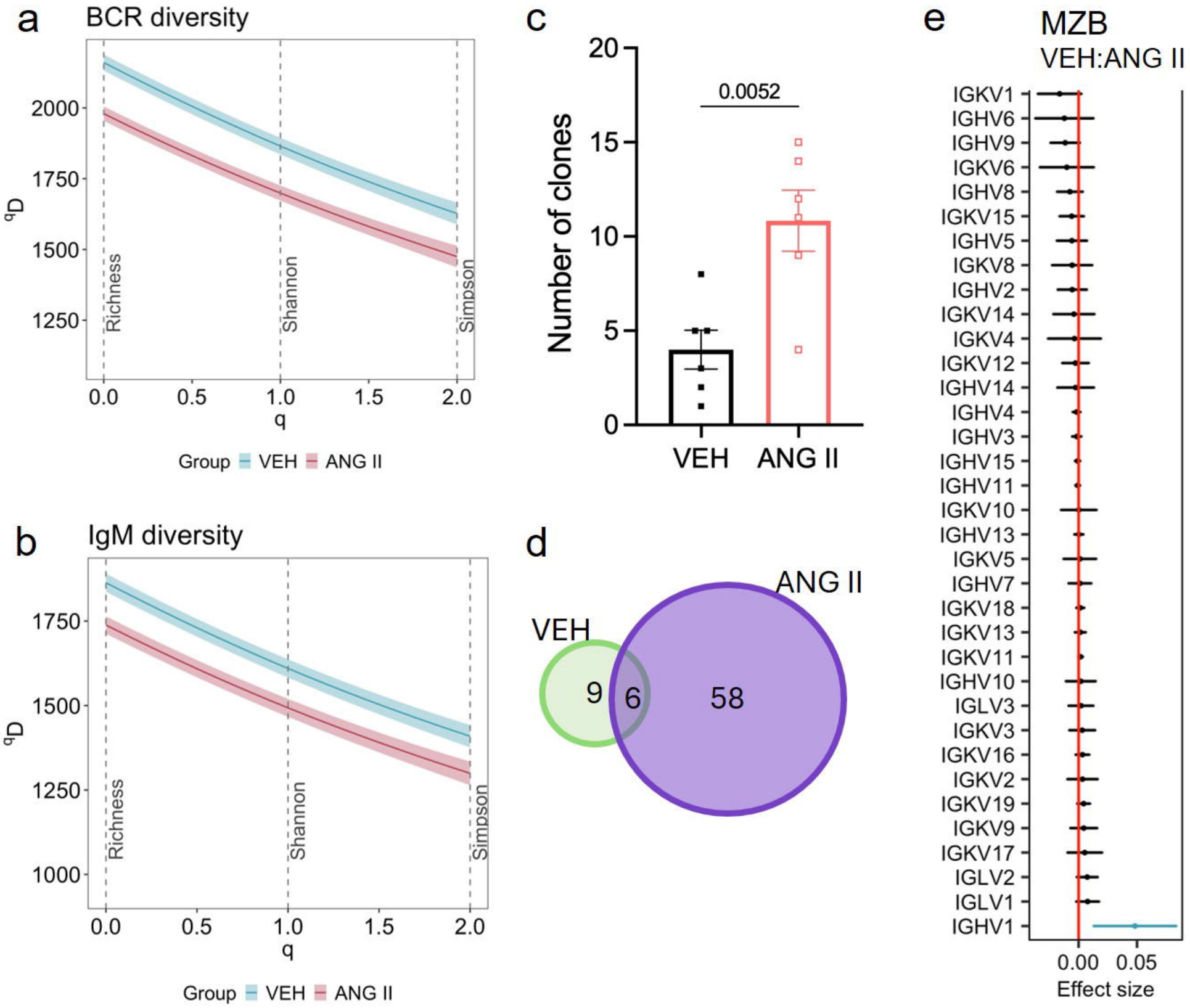
a
BCR diversity
2000
1750
1500
1250
qD
Richness
Shannon
Simpson
0.0
0.5
1.0
1.5
2.0
q
Group VEH ANG II
b
IgM diversity
1750
1500
1250
1000
qD
Richness
Shannon
Simpson
0.0
0.5
1.0
1.5
2.0
q
Group VEH ANG II
c
20
15
10
5
0
Number of clones
0.0052
VEH
ANG II
d
VEH
ANG II
9
6
58
e
MZB
VEH:ANG II
IGKV1
IGHV6
IGHV9
IGKV6
IGHV8
IGKV15
IGHV5
IGKV8
IGHV2
IGKV14
IGKV4
IGKV12
IGHV14
IGHV4
IGHV3
IGHV15
IGHV11
IGKV10
IGHV13
IGKV5
IGHV7
IGKV18
IGKV13
IGKV11
IGHV10
IGLV3
IGKV3
IGKV16
IGKV2
IGKV19
IGKV9
IGKV17
IGLV2
IGLV1
IGHV1
0.00
0.05
Effect size

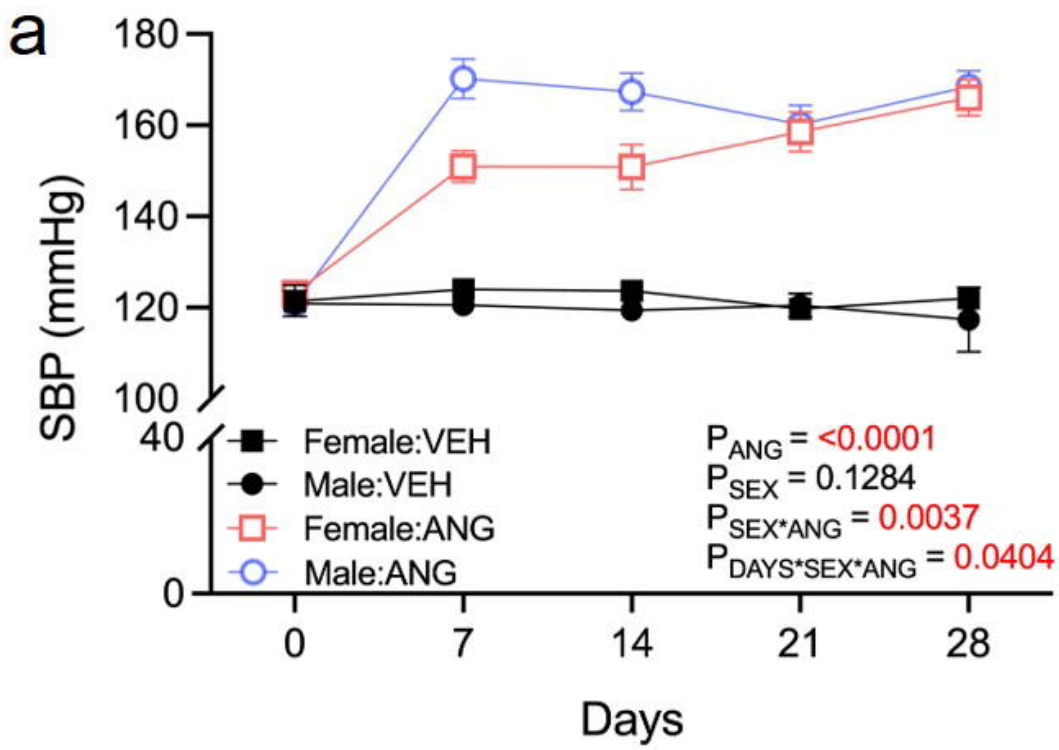

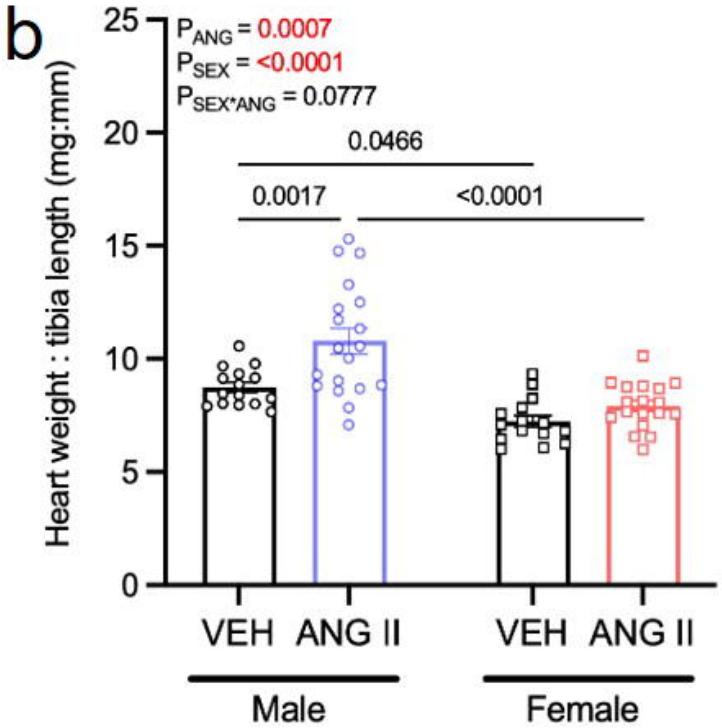

c

Organ	Population	Veh male	Veh female	Ang II male	Ang II female	P_{ANG}	P_{SEX}	$P_{ANG*SEX}$
Spleen	MZB	4.011±0.288	4.455±0.308	5.462±0.530	5.304±0.463	**0.0091**	0.7345	0.4774
	CD69+ MZB	0.003±0.001	0.005±0.001	0.006±0.001	0.008±0.002	**0.0211**	0.2416	0.9741
	Nur77+ MZB	0.034±0.007	0.020±0.003	0.045±0.008	0.037±0.004	**0.0129**	**0.0483**	0.5984
	CD27+ MZB	0.004±0.001	0.004±0.001	0.006±0.001	0.005±0.001	0.1964	0.6784	0.6843
Kidney	MZB-like	0.674±0.184	1.058±0.170	1.712±0.453	1.668±0.327	**0.0182**	0.6122	0.5247
	CD69+ MZB-like	0.022±0.007	0.032±0.009	0.074±0.021	0.063±0.015	**0.0091**	0.9745	0.4899
	Nur77+ MZB-like	0.043±0.013	0.033±0.006	0.125±0.030	0.082±0.029	**0.0139**	0.2959	0.5161
	CD27+ MZB-like	0.005±0.002	0.013±0.004	0.027±0.008	0.029±0.007	**0.0125**	0.506	0.6504

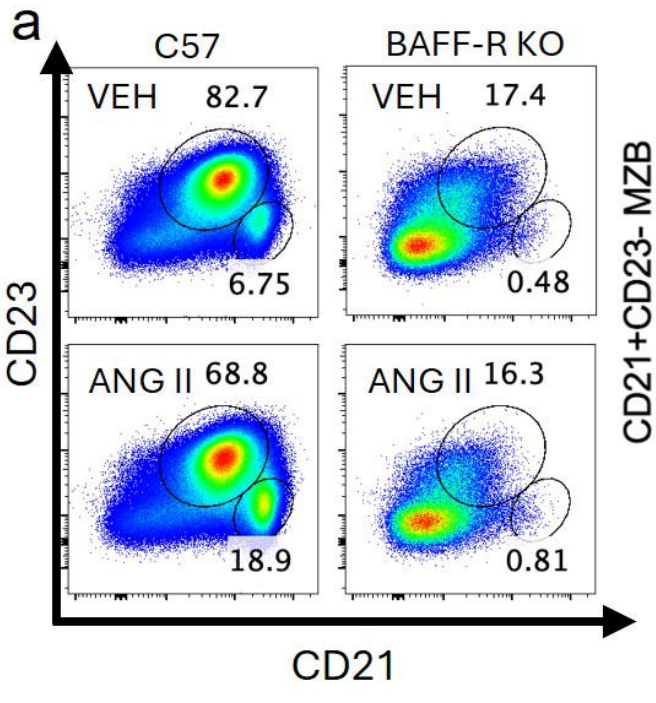
a
C57
BAFF-R KO
VEH
82.7
6.75
VEH
17.4
0.48
ANG II
68.8
18.9
ANG II
16.3
0.81
CD23
CD21

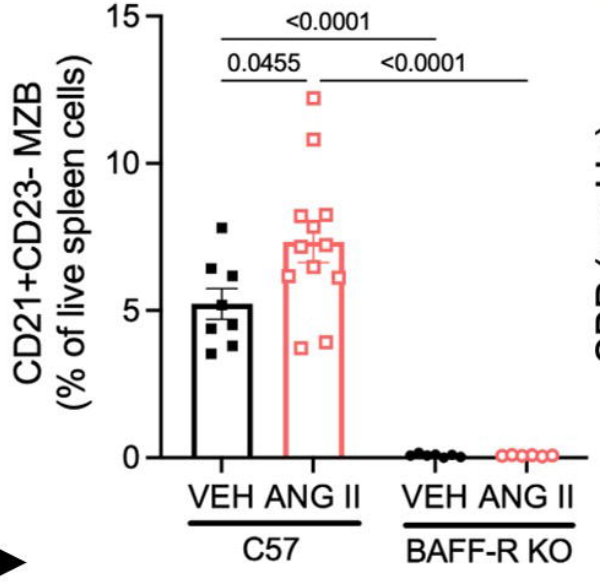
CD21+CD23- MZB
(% of live spleen cells)
15
10
5
0
<0.0001
0.0455
<0.0001
VEH ANG II
VEH ANG II
C57
BAFF-R KO

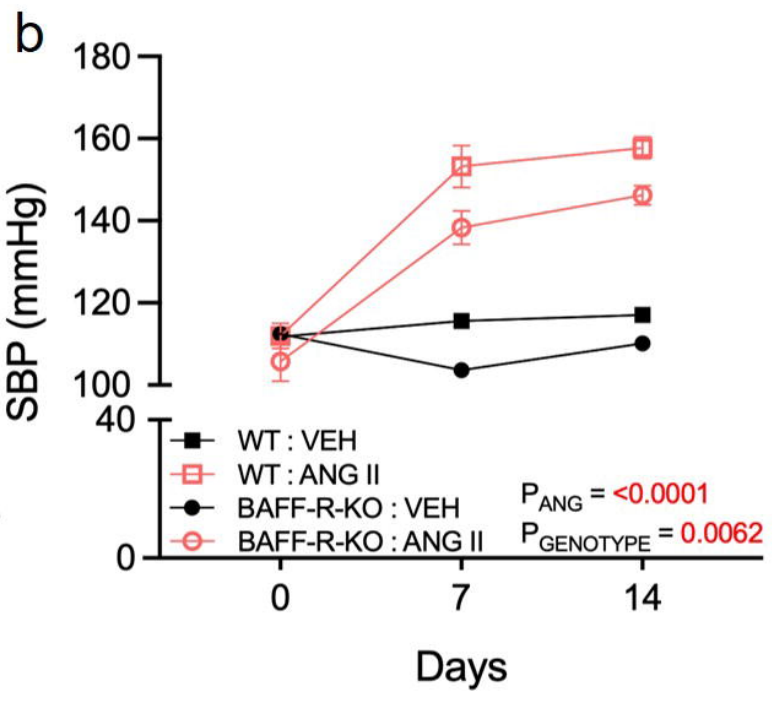
b
SBP (mmHg)
180
160
140
120
100
40
0
WT : VEH
WT : ANG II
BAFF-R-KO : VEH
BAFF-R-KO : ANG II
P_ANG = <0.0001
P_GENOTYPE = 0.0062
0
7
14
Days